ACIBADEM MEHMET ALI AYDINLAR UNIVERSITY
INSTITUTE OF HEALTH SCIENCES

FUNCTIONAL CHARACTERIZATION AND RECLASSIFICATION OF GENOMIC VARIANTS OF UNCERTAIN SIGNIFICANCE IN HEREDITARY CANCERS

SEVDİCAN ÜSTÜN YILMAZ
PH.D. THESIS

DEPARTMENT OF MEDICAL BIOTECHNOLOGY

SUPERVISOR
Prof. Uğur Özbek

SECONDARY SUPERVISOR
Prof. Meltem Müftüoğlu

ISTANBUL-2024

ACIBADEM MEHMET ALI AYDINLAR UNIVERSITY
INSTITUTE OF HEALTH SCIENCES

FUNCTIONAL CHARACTERIZATION AND RECLASSIFICATION OF GENOMIC VARIANTS OF UNCERTAIN SIGNIFICANCE IN HEREDITARY CANCERS

SEVDİCAN ÜSTÜN YILMAZ
PH.D. THESIS

DEPARTMENT OF MEDICAL BIOTECHNOLOGY

SUPERVISOR
Prof. Uğur Özbek

SECONDARY SUPERVISOR
Prof. Meltem Müftüoğlu

ISTANBUL-2024

DECLARATION

I declare that this thesis is my own work. I had no unethical behavior at any stage from the planning to the writing of the thesis. I obtained all the information in this thesis in accordance with academic and ethical rules. I cited all the information and comments that were not obtained with this thesis work, and I provided resources in the list of references. I also declare that there was no violation of any patents and copyrights during the study and writing of this thesis.

Date: 15.11.2024

PREFACE AND ACKNOWLEDGEMENT

TABLE OF CONTENTS

LIST OF ABBREVIATIONS AND SYMBOLS

γ	gamma
aa	Amino acid
ACMG	American College of Medical Genetics and Genomics
AMP	Association for Molecular Pathology
AT	Ataxia Telangiectasia
B/ LB	Benign/ Likely Benign
BLE	Bleomycin
BRCA1	Breast cancer gene 1
BRCA2	Breast cancer gene 2
BS3	Benign strong 3
ClinGen	Clinical Genome Resource
ClinVar	Clinical Variant database
D	Deleterious
dbNSFP	Database non-synonymous single-nucleotide variants functional prediction
DDR	DNA damage repair
Dox	Doxorubicin
DSB	Double Strand Break
gnomAD	The Genome Aggregation Database
H2AX	Histone H2AX
HBOC	Hereditary Breast and Ovarian Cancer
HR	Homologous recombination
HRR	Homologous recombination repair
NGS	Next-generation sequencing
P/ LP	Pathogenic/ Likely Pathogenic
PBMC	Peripheral Blood Mononuclear Cell
PolyPhen-2	Polymorphism Phenotyping v2
PS3	Pathogenic strong 3
SDM	Site directed mutagenesis
SIFT	Sorting Intolerant From Tolerant

SNV	Single Nucleotide Variants
SSB	Single Strand Break
SVI	Sequence Variant Interpretation
T	Tolerated
TP53	Tumor Protein P53
VarSome	The human genomic variant search engine
VUS	Variants of Uncertain Significance

LIST OF FIGURES

LIST OF TABLES

ABSTRACT

Functional Characterization and Reclassification of Genomic Variants of Uncertain Significance in Hereditary Cancers

BRCA1/2 germline likely pathogenic/pathogenic (LP/P) variations impact the onset of different malignancies. Hereditary cancer panel testing, with the contribution of Next-generation sequencing (NGS)-based technology, has advanced our understanding of hereditary breast and ovarian cancer (HBOC) genetics, revealing numerous variants of uncertain significance (VUS) whose impact on cancer development remains unclear. Our study's objective is to build a functional analytic methodology to ascertain the medical consequences of missense variations in the genes responsible for moderate and high-risk cancer susceptibility, respectively, *ATM* and *BRCA2*. We retrospectively scan the hereditary cancer panel testing results of 1200 cases, selecting five missense *ATM* and *BRCA2* VUSs, and performed in silico studies for further studies. In our first project on *ATM* c.7793G>A variant, we performed site-directed mutagenesis and analyzed *ATM* gene expression and ATM, CHEK2, and TP53 proteins, their phosphorylated forms and γH2AX levels before and after exposed to DNA-damaging agent bleomycin. Unfortunately, we did not observe any substantial variance among the assay groups. In our second project, we focused on *BRCA2* VUS and examined the variations in DNA damage through the utilization of comet and γH2AX assays on peripheral blood mononuclear cells (PBMCs) both before and after exposure to the DNA-damaging agent doxorubicin. Based on our merged studies, variants were reclassified and considered T1001R VUS-intermediate, T1104P/M1168K, D2819V VUS(+), R2027K, and G2044A likely benign. Our results underscore the significance of functional assays in understanding VUS impacts on cancer susceptibility genes. We aim to create a robust VUS analysis pipeline for clinical diagnostics, facilitating accurate variant classification and contributing to personalized cancer treatment strategies.

Keywords: Hereditary breast and ovarian cancer (HBOC) syndrome, VUS classification, ATM, BRCA2, Functional assays.

ÖZET

Kalıtsal Kanserlerde Klinik Önemi Bilinmeyen Genomik Varyantların Fonksiyonel Karakterizasyonu ve Yeniden Sınıflandırılması

BRCA1/2 germ hattındaki muhtemel patojenik/patojenik (LP/P) varyasyonlar farklı malignitelerin başlangıcını etkiler. Yeni nesil dizileme (YND) tabanlı kalıtsal kanser paneli test teknolojisi, kalıtsal meme ve over kanseri (KMOK) genetiğine ilişkin anlayışımızı geliştirerek, kanser gelişimi üzerindeki etkisi belirsiz kalan çok sayıda klinik önemi bilinmeyen varyasyonları (VUS) ortaya çıkardı. Çalışmamızın amacı, sırasıyla orta ve yüksek riskli kanser duyarlılığından sorumlu genler olan *ATM* ve *BRCA2*'deki anlamsız varyasyonların tıbbi sonuçlarını belirlemek için işlevsel bir analitik metodoloji oluşturmaktır. 1200 kişinin çoklu gen kanser paneli sonuçlarını geriye dönük olarak analiz ettik, beş hatalı *ATM* ve *BRCA2* VUS seçtik ve daha ileri çalışmalar için in silico çalışmaları gerçekleştirdik. *ATM* c.7793G>A varyantına ilişkin ilk projemizde, alan hedefli mutajenez gerçekleştirdik ve DNA'ya zarar veren ajan bleomisine maruz kalmadan önce ve sonra *ATM* gen ekspresyonu ile ATM, CHEK2, TP53 proteinleri ile bunların fosforile formları ve γH2AX düzeylerini analiz ettik. Maalesef test grupları arasında anlamlı bir fark bulamadık. İkinci projemizde *BRCA2* VUS'a odaklandık ve DNA'ya hasar veren ajan doksorubisin ile indüksiyon öncesi ve sonrasında PBMC'ler üzerinde comet ve γH2AX analizlerini kullanarak DNA hasarındaki değişiklikleri gözlemledik.. Kombine hesaplamalı ve fonksiyonel analizler, T1001R'nin VUS-orta seviye, T1104P/M1168K, D2819V'nin VUS(+) ve R2027K ve G2044A'nın muhtemelen iyi huylu olarak yeniden sınıflandırılmasına yol açtı. Bulgularımız, VUS'un kansere yatkın genler üzerindeki etkilerini anlamada fonksiyonel analizlerin öneminin altını çiziyor. Klinik teşhis için sağlam bir VUS analiz hattı oluşturmayı, doğru varyant sınıflandırmasını kolaylaştırmayı ve kişiselleştirilmiş kanser tedavisi stratejilerine katkıda bulunmayı hedefliyoruz.

Anahtar Sözcükler: Kalıtsal meme ve over kanseri (KMOK), VUS sınıflandırması, ATM, BRCA2, Fonksiyonel deneyler.

1 INTRODUCTION AND AIM

Personalized medicine is an approach developed to predict patient groups more accurately for a specific disease to which treatment and prevention strategies will be applied (1). It has grown considerably in recent years due to genetic counseling and comprehensive gene sequencing applications used routinely. The importance of personalized preventive treatment for hereditary cancers, especially hereditary breast and ovarian cancer (HBOC), has increased. 5-10 % of all cancer cases are hereditary and usually result from germline variations of genes that control the cell cycle or DNA damage repair (2, 3).

Targeted panels, whole exome, whole genome, and mitochondrial DNA sequencing tests detect germline variations in inherited diseases, especially preferred in immune system deficiencies, blindness, deafness, mitochondrial disorders, cardiomyopathies, and cancer predisposition syndromes (4). The developing next-generation sequencing (NGS) technology also enables the detection of many genomic variants with the high resolution it provides by analyzing many genes at once in a more accurate, fast, effective, and economical way (5).

In 2015, the American College of Medical Genetics and Genomics and the Association for Molecular Pathology Consensus (ACMG/AMP) published specific standards and guidelines for the interpretation of the obtained sequence variants in accordance with variants classified as benign/ likely benign (B/LB), pathogenic/ likely pathogenic (P/LP), or variants of uncertain significance (VUS) (6). To classify the obtained sequence variants under these categories, i) the allele frequency of the variant in disease and population databases (1000Genomes; ClinVar; GnomAD) and its incidence in affected individuals, ii) pathogenicity scores in *in-silico* prediction tools (CADD; MutationTaster; PolyPhen-2; Provean; SIFT), iii) segregation data, iv) functional data results should be taken into account (6).

Each variant carrier has an independent gene profile consisting of P (increasing the risk of cancer) or B (reducing the risk of cancer) variants, and the individual's

cancer risk is determined by combining the criteria in the ACMG/AMP classification. Additionally, in some profiles, the clinical impact of the variant in the individual at risk for cancer is unknown and is classified as VUS (7). As a result of NGS, VUSs are 40 % of the total detected variants, and we cannot identify their clinical significance (8).

Functional evidence codes make sense for the classification of VUSs; proving the variant effect with functional assays is essential. According to the ACMG/AMP criteria, "well-established" functional tests make an outstanding contribution to establishing the differences between the "wild-type" (wt) and variant forms of genes, allowing the variant to be reclassified by the change they create in scoring as pathogenic strong (PS3) or benign strong (BS3) (6). Studies on the functional characterization of variants differ depending on the type of variant analyzed (missense, splicing duplication/deletion, etc.), the protein region where it occurs, and the function it changes (9). These features include activity experiments depending on the gene's function, stability experiments depending on protein properties, immunoblot experiments where expression change is analyzed, etc., which can be designed differently.

Thus, in this study, we planned to combine gnomAD, ClinVar, and *in-silico* analysis results with homologous recombination (HR) pathway protein expression assays and measure damaged DNA before to and following exposure to DNA damage inducer chemotherapeutic drugs.

This study is unique because it will be the first to describe the functional consequences of selected *ATM* and *BRCA2* variants to prove their pathogenicity. We studied *ATM* variants inside the whole *ATM* gene with site-directed mutagenesis (SDM) experiments. In addition to the methods accepted in the literature, we were the first to apply the comet assay with peripheral blood mononuclear cells (PBMCs) of individuals has previously received a breast cancer (BC) diagnosis.

Considering our results, we aimed to create a VUS analysis pipeline. Thus, we aimed to develop a new and effective method to analyze other VUSs we encounter more quickly.

2 BACKGROUND

2.1 Types of Cancer

Cancer is a complex disease that occurs with uncontrolled cell growth and division of these cells and spreads to surrounding tissues and organs (10). Abnormal cell changes occur with gene mutations and can be inherited or acquired (somatic). Most of the cancer cases developed first in a germ cell or early embryogenesis of the fertilized egg due to a somatic mutation, referred to as sporadic (non-familial) cancers, occur with endogenous and exogenous DNA damage agents, damage of DNA, and consequent epigenetic DNA repair defects (11).

2.2 Hereditary Breast and Ovarian Cancer

Hereditary cancer accounts for 5-10 % of all cancers, is a germline mutation passing from parents to their children and among first- and second-degree relatives (12). Compared to sporadic forms of the same cancer type, hereditary cancers often occur at an early age of onset, are more aggressive, and are treated differently (13).

In 1990 and afterward, DNA linkage studies in HBOC were associated first with *BRCA1* (BC gene 1) and then in 1994 with *BRCA2* (BC gene 2) in DNA repair genes (14, 15). These inventions revealed the pathogenesis of HBOC and prognostic genetic testing usable for predicting cancer risk. In around 30 to 50 percent of people with an increased risk of HBOC, the oncosuppressor *BRCA1* (OMIM 113705) and *BRCA2* (OMIM 600185) genes are carriers of PVs (16).

BC risk is 12 % in the general population; this increases with germline pathogenic mutation 55-72 % by age 70 in *BRCA1* and 45-69 % in *BRCA2*; ovarian cancer (OC) risk is 1-2 % in the general population; this increases with germline pathogenic mutation 39-44 % and 11-17 % in *BRCA1* and *BRCA2*, respectively (17). For this reason, many clinicians and geneticists established the National Comprehensive Cancer Network (NCCN) to examine cancer-associated genetic

variants found in cancer patients and family members, regulate the risk of disease, and recommend steps to reduce this risk, such as chemotherapy, mammography, risk-reducing mastectomy, etc. (18, 19).

BRCA1 and *BRCA2* gene PVs are the most relevant genetic mutations associated with HBOC, except some other genes also have PVs that elevate the risk of BC and OC (20). The last few decades have proven that tumor suppressors and DNA damage repair gene families are responsible for this syndrome. These highly penetrated genes are *TP53* (Li-Fraumeni syndrome) (21), *CDH1* (Hereditary diffuse gastric cancer) (22), *STK11* (Peutz-Jeghers syndrome) (23), and *PTEN* (Cowden syndrome) (24) tend to a kind of different cancers but have a high risk of BC (Table 1).

Table 1 Highly-penetrated genes linked to syndromes and neoplasms related to BC and OC.

Genes	Syndrome	Locus	Neoplasm
BRCA1	Hereditary Breast / Ovarian Cancer Syndrome (HBOC)	17q12-21	Female BC, OC, contralateral BC
BRCA2	HBOC	13q12-13	Male and female BC, OC, contralateral BC, prostate
TP53	Li-Fraumeni syndrome	17p13.1	BC, Soft tissue sarcomas, osteosarcoma, brain ca.
PTEN	Cowden syndrome	10q23.3	Female BC, thyroid, endometrial ca.
STK11	Peutz-Jeghers syndrome	19p13.3	BC
CDH1	Hereditary gastric cancer	16q22.1	Hereditary diffuse gastric ca., female BC
BC: Breast Cancer, OC: Ovarian Cancer, ca: cancer			

Moderate-penetrated BC genes are *PALB2*, *NBN*, *CHEK2*, and *ATM* (25-28) (Table 2). On the other side, *MLH1*, *MSH2*, *MSH6*, and *PMS2* (Lynch syndrome) gene mutations, besides those *BRIP1*, *RAD51C*, and *RAD51D*, are the genes that have a high-risk factor for OC development (29-32) (Table2).

Table 2 Moderate and low-penetrated genes linked to syndromes and neoplasms related to BC and OC.

Genes	Syndrome	Locus	Neoplasm
ATM	Ataxia-Telangiectasia	11q22.3	BC and OC
BARD1	BARD1 related	2q34-q35	BC and OC
BRIP1	Fanconi Anemia	17q22-q24	BC
PALB2		16q12.1	OC and Female BC
CHEK2	CHEK2 related	22q12.1	BC and OC
MLH1	Lynch syndrome	3q22.2	BC and OC
MSH2		2p21-p16	OC
MSH6		2p16.3	OC
PMS2		7p22.1	OC
EPCAM		2p21	Colorectal and endometrial ca.
NBN	Nijmegen Breakage Syndrome	8q21.3	BC
NF1	Neurofibromatosis Type I	17q11.2	BC
RAD51C	RAD51 related	17q22	Epithelial OC
RAD51D		17q12	OC
BC: Breast Cancer, OC: Ovarian Cancer, ca: cancer			

2.3 DNA Damage Pathway and the Role of BRCA2 and ATM

Several intrinsic and extrinsic factors cause DNA damage and genomic instability in cells, which are protected by stalling the cell cycle, triggering cellular death, and activating DNA repair mechanisms (33). Depending on the cause of the damage, single-strand breaks (SSBs) or double-strand breaks (DSBs) occur on the DNA, and the second one is more destructive if it is not repaired correctly and causes mutations (34). HR and non-homologous end-joining (NHEJ) repair pathways play roles in repairing DSBs, based on the cell cycle's present state (35).

The HR repair pathway occurs only during the cell cycle's late S and G2 phases. For this pathway to work, a healthy homologous DNA sequence must be present in the sister chromatin, which will be used as a template for the synthesis of the damaged region (36). The process begins with the MRN complex, consisting of Mre11, RAD50, and Nbs1, identifying the DSB region. Subsequently, ATM is brought to the site of DNA damage, which helps to recruit other essential proteins like ATR, CHEK2, BARD1, BRCA1, BRCA2, and RAD51 (36). If components of the HR pathway are defective, the less sensitive NHEJ repair pathway acts as a backup and activates mainly in the G0 and G1 phases (36).

2.3.1 BRCA2

The BRCA2 genomic region is found on chromosome 13 and is 84 kb in size. It comprises 27 exons and encodes a 3418 aa (amino acid) nuclear protein (37). This protein has four different domains: the N-terminus mediates interactions with PALB2 (Partner and Localizer of BRCA2), the central BRC repeat area mediates interactions with RAD51, the “DNA-binding domain” (DBD) with three tandem “oligonucleotide/oligosaccharide-binding folds” (OB-folds) and lastly the C-terminal domain (CTD) (37).

By controlling the HR repair (HRR) pathway, BRCA2 contributes to the repair of DNA damage via connecting with DNA-repairing proteins RAD51 and

phosphorylating histone H2AX (γH2AX) (36). γH2AX recruits DNA repair factors to the damaged site, potentiates the HRR of DNA DSBs, and links the chromatin remodeling process to DNA repair (37). BRCA2 repairs damaged DNA and suppresses cancer by interacting with RAD51 recombinase for HRR in cells (38). The HRR pathway related to BRCA2 occurs through the interaction of BRCA2 and RAD51 in two different regions; the BRC repeat region in exon 11 which is also interacts with PALB2/FANCN, which enables BRCA1 to bind to BRCA2 and a single domain in the exon 27 (39, 40). In human cells, BRCA2 loss causes homology-directed repair (HDR) deficiencies, genome destabilization, micronuclei development, decreased fork protection after replication stress, defective RAD51 foci formation after DNA damage, and chemotherapeutic susceptibility (41).

2.3.2 ATM

Ataxia-telangiectasia (AT), caused by a mutation in the *ATM* gene, is an autosomal recessive, neurodegenerative disease and is characterized by immunodeficiency, progressive cerebellar ataxia, radiosensitivity, sensitivity to DNA damage, cell cycle checkpoint defects, and cancer susceptibility (42). ATM, activated by agents that create DSBs in DNA, such as ionizing radiation, phosphorylates p53, CHEK2, and BRCA1, which are in the downstream of the same pathway, and as a result, variants in *ATM* or these genes cause cancer predisposition (43).

The *ATM* gene encodes a 350 kDa protein kinase enzyme containing 66 exons in the 11q22-23 chromosome region (44). ATM protein belongs to the phosphatidylinositol-3' kinase (PI3K)-related protein kinase family and is involved in DNA DSB repair and the cell cycle (45). ATM phosphorylates other proteins in the pathway of DNA damage and cell cycle control by autophosphorylation, and with the transphosphorylation, monomerizes and partially activates the dimer form of itself after the DNA DSBs and causes changes in the chromatin structure (46). Full activation of ATM occurs by binding to the MRE11-RAD50-NBS1 (MRN) (45). As a result of DNA breakage, inactive ATM dimers, via the MRN complex, cause ATM

to be cleaved into Ser1981 auto-phosphorylated active monomers and act on its substrates, such as TP53 or H2AX (45). These events are critical indicators of ATM functional activity, and the coordinated activity of phosphorylated downstream signaling pathway targets determines whether genomic instability resulting from DNA damage can be prevented (47).

In the literature, studies have observed that cells of patients with AT phenotype cannot perform ATM kinase activity and, therefore, cannot express ATM protein (48). In contrast, patients with a milder AT phenotype have reduced ATM kinase activity and regular ATM protein expression (49). AT patient cells are highly sensitive to ionizing radiation and agents that cause DSBs, leading to a decrease in ATM Ser1981 phosphorylation (50), a decrease in the survival mechanism, an increase in the rate of chromosomal abnormalities, and damage to cell cycle checkpoints (51, 52). On the other hand, some missense variants allow ATM expression but lead to residual kinase activity (53, 54).

2.4 Genetic Testing

Genetic testing helps understand the risk of developing cancer in an individual with a cancer predisposition family history or inherited gene mutations and the risk of developing other cancers for a cancer patient (55). Genetic counseling, screening, and prevention improve the risky individual's future with the genetic testing results and affect the onset of cancer or the disease's sequela (55).

Genetic sequencing has improved with the development of technology and empowers accurate, quicker, and cheaper parallel sequencing of multiple genes simultaneously (5). Several commercial and noncommercial NGS-based gene panel tests have been introduced to clinicians to find genetic mutations that affect medical management (56). If one gene is associated with an inherited cancer syndrome or a patient has a history in agreement with inherited cancer susceptibility, then multigene panel testing becomes useful (57). Additionally, panel testing result in a 3 % rise in the incidence of variations in other genes linked to the susceptibility to BC and OC in

individuals with a strong personal and family history and negative *BRCA1/2* test findings (58).

However, this technology brings out new challenges, such as determining new genes to constitute a genetic panel, managing the patients with an unknown penetrance of a gene, managing an enhanced number of VUS, and finding a random mutation with an unknown phenotype in the family history (59).

2.5 Variants of Uncertain Significance

Each variant carrier has a different gene profile associated with pathogenic or benign variants, which increase or decrease the person's cancer risk. In some profiles, the impact of the causality of variants in cancer-risk individuals is unknown and classified as VUS (7). In the Multidimensional Impact of Cancer Risk Assessment (MICRA) scale, genetic test-specific effects were reported higher in the VUS-reported patients than in negative patients and lower than in positive patients (60). VUS classification is difficult because they need more statistical evidence about the population, there is a lack of functional evidence, and researchers' assessments are different (8). In-vitro test evaluation should be supported by clinical databases and predictive biochemical algorithms, and genetic testing on family members is recommended for VUS (re)classification (8).

2.6 Variant Annotation and Classification

The ACMG/AMP guidelines standardized variant interpretations in 2015 and released criteria that take into account the variation's parental origin, its frequency in the population, in-silico predictions, functionality, and familial segregation data (6). According to the guidelines, PVs are evaluated with “very strong (PVS1), strong (PS1-4), moderate (PM1-6), or supporting (PP1-5)” evidence codes, and BVs are evaluated with “stand-alone (BA1), strong (BS1-4), or supporting (BP1-7)” evidence codes (6).

2.6.1 Computational databases

To classify the obtained sequence variants under ACMG/AMP categories, i) allele frequency of the variation in demographic and illness databases, as well as how frequently it appears in afflicted people, ii) pathogenicity scores in in-silico prediction tools, iii) segregation data, iv) functional data results should be taken into account.

2.6.1.1 ClinVar

ClinVar is an openly accessible and publicly available repository of human genetic variations and their associations with diseases and other medical conditions and is managed by the National Institutes of Health (NIH) (61). The submitted variations' interpretations are collected and can be accessed on the ClinVar website (62).

Based on data from the ClinVar collection as of April 2024, VUS accounts for over 50 percent of the inherited gene variations that predispose to cancer. In the *BRCA2* gene, there are 13820 single nucleotide variations (SNV), which include 8187 missense molecular consequences, and 7770 of them are VUS. In the *ATM* gene, there are 13329 SNV, which include 7256 missense molecular consequences, and 7133 of them are VUS.

2.6.1.2 Genome aggregation database

The Genome Aggregation Database (gnomAD), formerly known as the Exome Aggregation Consortium (ExAC), was established in 2014 by a group of researchers who agreed to collaborate and share combined exome and genome sequencing data from various extensive sequencing initiatives (63). The aim was to provide summary data to the broader scientific community. The gnomAD resource can be a valuable reference for studying allele frequencies in severe pediatric diseases. However, it is important to acknowledge that certain individuals with severe diseases may still be

present in the data sets, such as biobanks. Nevertheless, their inclusion is expected to be either equivalent to or less frequent than what is observed in the general population. In 2024, a dataset consisting of 76,156 human genomes from the gnomAD was utilized to construct a comprehensive genomic constraint map for the whole human genome and became the largest publicly accessible reference dataset containing allele frequency information for human genomes (64).

2.6.1.3 The human genomic variant search engine

The human genomic variant search engine, VarSome, is a multifunctional platform that serves as an online search engine, aggregator, and impact analysis resource for studying human genetic variation (65, 66). It is also a collaborative effort that aims to facilitate the exchange of global expertise on human variants (65).

2.6.1.4 Deciphering mutations in actionable genes

DeMAG (deciphering mutations in actionable genes) variants effect predictor tool is used to collect more information about the variants from global experts (67). This supervised classifier was developed utilizing a comprehensive dataset from 59 disorder genes with medical consequences provided by the ACMG Secondary Findings v2.0. DeMAG specifically focuses on missense variations and utilizes evolutionary and structural relationships among residues. Scores greater than or equal to 0,5 are classified as pathogenic.

2.6.1.5 Franklin

Franklin serves as a central point of connection within the field of medical genetics and generates a network effect that expands the actionable genomic information that influences patients' care. Franklin is compatible with all suppliers and workflows, allowing genetic professionals to provide more precise and meaningful data insights (68).

2.6.2 Computational prediction tools

The dbNSFP database algorithms consider the alterations in non-synonymous aa in the genes likely to affect gene functioning. Taking into account the results in this database, variants were analyzed with in-silico prediction tools to see the variant's pathogenicity on the protein level, such as SIFT, PolyPhen-2, and MetaRNN (69-71).

2.6.2.1 Sorting intolerant from tolerant

The Sorting Intolerant From Tolerant (SIFT) score is a predictor of whether the substitution of an aa will have an impact on the function of the protein (72). If the score close to 0 it is deleterious (D), on the contrary if it is close to 1 it is tolerated (T).

2.6.2.2 Polymorphism phenotyping

The PolyPhen-2 (Polymorphism Phenotyping v2) is a method that predicts the potential influence of an aa substitution on the structure and function of a human protein based on simple physical and comparative factors (73). If the score close to 1 it is deleterious (D), on the contrary if it is close to 0 it is tolerated (T).

2.6.2.3 Meta recurrent neural network

MetaRNN can predict the pathogenicity of human nonsynonymous SNVs by combining data from 28 different high-quality annotation scores using the repository of dbNSFP regarding 16 functional predictive rankings, SIFT, Polyphen2, etc. (69). MetaRNN rankscores range from 0 (tolerated) to 1 (damaging).

2.6.2.4 BayesDel

BayesDel refers to a meta-score used to assess deleteriousness, with an enhanced evaluation of the biological significance of genes to the disease, a modified linkage

analysis, a unique test for association with uncommon variants, and a transformed variant call quality score (74). The range of the score is 0,75731 to -1,29334. The likelihood that the variation is pathogenic increases with score. In order to maximize sensitivity and specificity in the classification of ClinVar variations, a standard threshold score (0,0692655 with MaxAF, -0,0570105 without MaxAF) was determined. There are two sets of BayesDel values in this database: one with integrated MaxAF and one without (74).

2.6.3 Functional data

In 2015, the ACMG/AMP consensus standards and guidelines were used to establish criteria for evaluating clinical sequencing variations. They included strong evidence codes “PS3 and BS3” for "well-established" functional tests, and this evidence demonstrates the protein function of normal or abnormal genes (6). However, these evidence codes cause a variant interpretation inconsistency between laboratories lacking detailed guidance for evaluating a functional assay. For this reason, the Clinical Genome Resource (ClinGen) Sequence Variant Interpretation (SVI) Working Group presents a more consistent framework to determine clinical variant interpretation and constitute strengthful assay validation (75).

2.7 Functional Assays for VUS Classification

Functional laboratories require an efficient workflow for the evaluation of VUS. They should constitute a workflow for each gene and separate the assay of missense, splicing, and gross duplication VUS from each other depending on the variation type (9).

Until now, the *BRCA1* and *BRCA2* genes have been the focus of several functional analyses in the scientific literature (76, 77). Individualized therapies and the rise in VUS have made these trials even more important (8). In-vitro studies with poly (ADP-ribose) polymerase (PARP) inhibitors (PARPi) have shown effectiveness in the treatment of breast and OC carriage mutations not only in *BRCA1/2* but also in

DNA damage HR pathway-associated genes, such as *PALB2*, *RAD51*, *ATM*, *ATR*, and *CHK2* (78, 79). Generally, choosing the type of in vitro assay should consider the method that will be useful in measuring essential functions in carcinogenesis and identifying the variant's pathogenesis; however, because of their unclear biochemical roles, the *BRCA1* and *BRCA2* genes provide a challenge to overcome.

Studies employing in-vitro test techniques design them based on the sort of mutation, the animal model to be utilized, the location of the mutation in the protein, and the altered function (8). Until now, HDR tests (80, 81), in vitro transactivation of particular regions (82), and ubiquitin ligase efficiency assessment (83) have mainly been studied methods. In mutated cell lines, micronucleus formation and centrosome amplification are other types of assays (84, 85). Also, some studies measured splicing defects by minigene construction or DNA transcripts (86, 87). New genome editing technologies pave the way for more useful and robust assays that allow direct manipulation of gene sequences to observe the biological effects of SNVs in specific protein regions with multiplexed experiments (88). Saturation genome editing is a vital assay, especially using the CRISPR/Cas9 technology, which was improved by Findlay et al. (89).

All these functional assays still have some problems, mainly when used in daily clinical practice. Using an experimental method that belongs to commercial cell lines is also time-consuming. Gene editing cannot be usable in different kinds of variants and genes. Despite all these problems, functional assays show tangible efficacy in VUS classification, and research techniques are required for categorizing genetic variations linked to cancer.

3 MATERIALS AND METHODS

3.1 Materials and Solutions

Table 3 Materials used in the comet assay

Materials supplied from the kit
Lysis solution
Comet LMAgarose (LMA)
Trevigen CometSlide
200 mM EDTA, pH 10
Reagents used in the comet assay
Deionized water
10X PBS, Ca/Mg free
95 % Ethanol
TE buffer (10 mM Tris (pH 7,5), 1 mM EDTA)
10000X SYBR Gold in DMSO
NaOH pellets
0,5 M EDTA (pH 8.0)
Alkaline unwinding solution: pH > 13 (200 mM NaOH, 1 mM EDTA)
Alkaline electrophoresis solution: pH > 13 (200 mM NaOH, 1 mM EDTA)

Table 4 Protein analysis buffers

RIPA: 50 mM Tris-HCl, 150 mM NaCl, 0,5 M EDTA, 1 mM NaF, 1 mM Na_3VO_4, 0,5 % NP-40, 20 % Triton X-100, 0,5 mM PMSF, 1 mM DTT, 1X Phosphatase Protease inhibitor, dH2O
5X Laemmli: 1,75 ml 0,5 M Tris-HCl pH 6,8, 4,5 ml glycerol, 0,5 g SDS, 0,5 ml 0,25 % Bromophenol blue, 1,25 ml β-mercaptoethanol
Running: 25 mM Tris base, 190 mM Glycine, 0,1 % SDS, pH to 8,3
Transfer (Blotting) for HMW proteins: 5,8 g Tris, 2,9 g Glycine, 0,3 g SDS, H2O up to 1000 ml, add < 10 % Methanol freshly
1X TBS (washing): 2,42 g Tris base, 8,8 g NaCl, pH 7,6 with HCl, H2O up to 1000 ml
1X TBST (washing): 1000 ml TBS, 1 ml Tween-20
5 % Blocking: 5 % non-fat milk, 1X TBST or 5 % BSA, 1X TBST
Stripping: 12,5 ml 0,5 M Tris-HCl pH 6,8, 20 ml 10 % SDS, 0,8 ml β-mercaptoethanol, H2O to 100 ml

Table 5 List of antibodies

Antibody	Company	Catalog #
Phospho-Histone H2A.X (Ser139) (20E3) Rabbit mAb	CST	9718S
beta-Actin (8H10D10) Mouse mAb	CST	3700S
Anti-mouse IgG, HRP-linked Antibody	CST	7076S
Anti-rabbit IgG, HRP-linked Antibody	CST	7074S
ATM Monoclonal Antibody	Invitrogen	MA123152
Phospho ATM (Ser1981) Antibody	Affinity	AF4120
Phospho CHK2 (Thr68) Antibody	Affinity	AF3036
Chk2 (D9C6) XP® Rabbit mAb	CST	6334S
Phospho-p53 (Ser15) (E9Y4U) Rabbit mAb	CST	82530S
p53 (1C12) Mouse mAb	CST	2524S

3.2 Company and Catalog Numbers

Table 6 Kits and chemicals

Kits and chemicals	Company	Catalog #
Advanced RPMI 1640 medium	Gibco	12633012
DMEM medium	Gibco	11965084
Heat-inactivated fetal bovine serum (FBS)	Gibco	10500064
Penicillin-Streptomycin	Biological Ind.	03-031-5B
DPBS w/o Ca, Mg	Invitrogen	14190094
Phosphate Buffered Saline (PBS)	Invitrogen	70011044
PBS with Tween (PBST)	CST	9890S
Isopropanol	PanReac AppliChem	A3928
Trypan blue	Sigma Aldrich	T8154
PureLink HiPure Plasmid Filter Maxiprep Kit	Invitrogen	K210017
Fugene HD Transfection Reagent	Promega	E2312
Ficoll-Paque Plus	Cytiva	17-1440-02
LB Broth	Merck	110285.0500
LB agar	Merck	110283.0500
NZY Broth	Thermo Fisher	13635-032
Ampicillin 100 mg/mL	Sigma-Aldrich	A5354
Trypsin EDTA Solution C	Biological Ind.	03-054-1B
Ethanol	Millipore	K50322786826
Methanol	Merck	106009
RNeasy Plus Mini Kit	Qiagen	74136
RevertAid First Strand cDNA Synthesis Kit	Thermo Scientific	K1622

Table 6 Kits and chemicals (continues)

QuantiTect SYBR green PCR Kit	Qiagen	204143
Agarose	Sigma-Aldrich	05066-500G
1 KB DNA ladder	Genemark	GLM11
DNA Loading Dye	Stemcell	79018
50X Tris/Acetic Acid/EDTA (TAE) Buffer	BioRad	1610773
Ethidium bromide solution	Sigma-Aldrich	E1510-10mL
Single-cell gel electrophoresis (Comet) Assay Kit	R&D Systems	4250-050
SYBR Gold Nucleic Acid Gel Stain	Invitrogen	S11494
Pierce™ ECL Western Blotting Substrate	Thermo Scientific	32109
Ponceau S Staining Solution	Thermo Scientific	A40000279
NP-40 Surfact-Amps™ Detergen	Thermo Scientific	28324t
PMSF Protease Inhibitor	Thermo Scientific	36978
DTT (Dithiothreitol)	Thermo Scientific	R0861
Pierce Protease and Phosphatase Inhibitor Mini Tablets	Thermo Scientific	A32959
30 % Acrylamide/Bis Solution, 37,5:1	BioRad	1610159
Doxorubicin 5 mg	CST	5927S
Bleomycin Sulfate	BioShop Canada	BLE011.10
Geneticin (G418 Sulfate)	BioShop Canada	GEN418.500
IPTG	GoldBio	I2481C
X-Gal	Bio Basic	BB0083
QuikChange II XL site-directed Kit	Agilent	200522
Skim milk (non-fat powder)	BioShop Canada	SKI400.250
CutSmart Buffer	NEB	B7204S
Sma I	NEB	R0141S
BamHI	NEB	R3136
HindIII	NEB	R3104
PageRuler plus prestained protein ladder	Thermo Scientific	26619
Ammonium persulfate (APS)	BioRad	1610700
Sodium dodecyl sulfate (SDS)	Sigma-Aldrich	436143
Coomassie blue dye	BioRad	161-0803
Dimethyl sulfoxide (DMSO)	Sigma-Aldrich	D2650
Glycerol	Merck	104057
Nuclease free water	NEB	B1500S
TEMED	Sigma Aldrich	T22500
Tween 20	Merck	822184
Tris	BioShop	TRS001.1
Glycine	Merck	100590
Triton	Neofroxx	1139ML500
Bradford Reagent	BioRad	5000205
Bovine Serum Albumin (BSA)	Sigma	A2153

Table 7 Equipment and consumable list

Equipment	Company and Catalog Number
Class II Biological Safety Cabinet	Thermo Scientific Safe 2020
Light microscope	Leica DM500
Fluorescence microscope	Zeiss Axio
CO2 Incubator	Thermo Scientific Heratherm
Water purification system	Merck Millipore Milli-Q® Advantage A10
pH meter	Thermo Scientific Orion Star A211
Magnetic shaker with heater	Thermo Scientific CIMAREC
Water bath	EMCO ESM-3710
Centrifuge	Beckman Coulter Allegra 64R
Centrifuge	Thermo Scientific SL16R
Microcentrifuge	Thermo Scientific MICROCL 21R
Vortex/ Mini-centrifuge	BioSan FVL2400N
Shaker	Witeg RK-2D
Dry block heating thermostat	BIOSAN Bio TDB-100
Automated cell counter	BioRad TC20
Cell counting slides	BioRad 1450011
Pipette aid	Isolab LB.IS.010.01.005
Pipettes (10, 100, 200, 1000 µl)	Thermo Scientific
Syringe filters 0,45µm-0,22µm)	Sartorius
Cell culture dishes	TPP
Cryogenic vials	Thermo Scientific
Flask	TPP
Loop	Thermo Scientific
Cell spreader	Isolab 082.03.001
Centrifuge tubes	Isolab
Fridge (+4º C)	Kirsch
Fridge (-20º C)	Arctıko LTFE370
Freezer (-80º C)	Haier Bio-Medical
Cryogenic storage	Themo Scientific Cryoplus2
Autoclave	Witeg and Nüve
Dry heat sterilizator	Nüve FN120
Liquid nitrogen tank	Arpege170
NanoDrop UV-Vis Spectrophotometer	Thermo Scientific ND-ONE-W
ChemiDoc™ Imaging System	BioRad MP
Thermal Cycler	BioRad T100
Real-Time PCR System	BioRad CFX96
Electrophoresis system	BioRad Mini Protean
Power supply	BioRad Power Pac Basic

Table 7 Equipment and consumable list (continues)

Ultrasonic homogenizer (sonicator)	Omni-Ruptor 4000
Incubator	Nüve
Spectrophotometer microplate reader	BioTek PowerWave XS2
Microwave	Samsung
Precision balance	Shimadzu UW620H
PVDF Membrane	BioRad 1620177
Mini PROTEAN tetra hancast system	BioRad 1658001FC
10-mL EDTA tubes	BD Vacutainer 366643
Blot paper filter paper	BioRad 1703956

3.3 Methods

3.3.1 Ethics committee approval

The studies were approved by the Acibadem Mehmet Ali Aydinlar University (ACU) and Acibadem Healthcare Institutions Medical Research Ethics Committee (ATADEK) (approval no. 2023-10/437 and 2021-11/06). They were performed following human research guidelines (Appendix 1 and 2). All subjects involved in the study provided their written informed consent according to the Declaration of Helsinki, as approved by the Ethics Committee of ACU and ATADEK (Appendix 3). All participants were informed about the present study, and written informed consent was obtained before participation in this study. All personal data was anonymized, and the samples were coded.

3.3.2 Filtering the panel test results

We partnered with “Istanbul Umraniye Training and Research Hospital Genomic Laboratory of Hereditary Cancer Clinic, Türkiye” (90) and “Acibadem Maslak Hospital Department of Medical Genetics, Istanbul, Türkiye” to obtain reports that we analyzed retrospectively between November 2017 and June 2022 (16). We found 1200 cases based on hereditary cancer panel findings of index individuals or subjects with a positive family history.

Medical Geneticists at both hospitals reviewed patients' medical and family histories before and after genetic testing, using the NCCN version when the patients were seen (18, 19) and ACMG/AMP guidelines (6). Hereditary cancer genetic testing reports were performed on the "*APC, ATM, BARD1, BRCA1, BRCA2, BRIP1, CDH1, CHEK2, EPCAM, FAM175A, MLH1, MRE11, MSH2, MSH6, MUTYH, NBN, PALB2, PMS2, PTEN, RAD50, RAD51C, RAD51D, STK11, TP53* and *XRCC2"* genes.

The cases with *ATM* and *BRCA2* variants were searched in the ClinVar database (91) We were grouped according to clinical consequences such as B/LB, VUS, P/LP, conflicting interpretations of pathogenicity (CIP), and not-reported (NR). We chose VUSs, CIP, and NR variants for the study and filtered missense SNVs.

3.3.3 Case selection

We received medical data from our partner hospitals of the individuals with the identified missense SNVs. To ensure their participation, we included women with a history of BC and OC who lacked additional mutations linked to a different inherited cancer-associated gene. We excluded some of the individuals from the studies according to some rules. After selecting the variants, we performed the in-silico analyses using the dbNSFP and other databases.

3.3.4 Data collection about variants

The Varsome human genomic variant search engine (65), DeMAG (deciphering mutations in actionable genes) variants effect predictor tool (67), and Franklin genetic evidence database (68) were used to collect detailed information about the variants from global experts.

We used dbNSFP database algorithms to consider the alterations in non-synonymous aa in the *BRCA2* and *ATM* genes likely to affect gene functioning. Taking into account the results in this database, variants were analyzed with in-silico

prediction tools to see the variant's pathogenicity on the protein level, such as SIFT (72), PolyPhen-2 (73), BayesDel (addAF and noAF), and MetaRNN (69-71). Variant population frequencies were collected from gnomAD version v4.0.0 (92).

3.3.5 Variant selection in the projects

3.3.5.1 ATM project

After filtering the *ATM* variants, we collected their computational results and chose variants prone to pathogenicity. We also collected the clinical information of these variant carriers, and some were excluded from the study for reasons such as being male, not having HBOC, or having variations in other genes. We also excluded some that might cause technical problems in the SDM experiment.

3.3.5.2 BRCA2 project

Clinical information on the *BRCA2* variant carriers was collected. Some were excluded from the study for reasons such as being male, lost to follow-up, not having HBOC, having variations in other genes, having travel problems, dying, or not wanting to participate. The detailed oncological disease history of each participant and their relatives was collected. Also, participants answered a questionnaire when they visited the clinic.

3.3.6 Experimental methods of the ATM project

3.3.6.1 Isolation and verification of the plasmid

The “pcDNA3.1(+)Flag-His-ATM-wt was a gift from Michael Kastan”. “Addgene plasmid #31985; http://n2t.net/addgene:31985; RRID: Addgene_31985” (93) (Figure 1). Plasmid shipped us from Addgene in stab culture format. After delivery, we streaked bacteria onto an LB agar/Amp plate. After ON growing at 37˚C, single colonies were isolated from the plate. Isolated single colonies were inoculated into the LB/Amp liquid culture at 37˚C and 250 rpm shaker incubator.

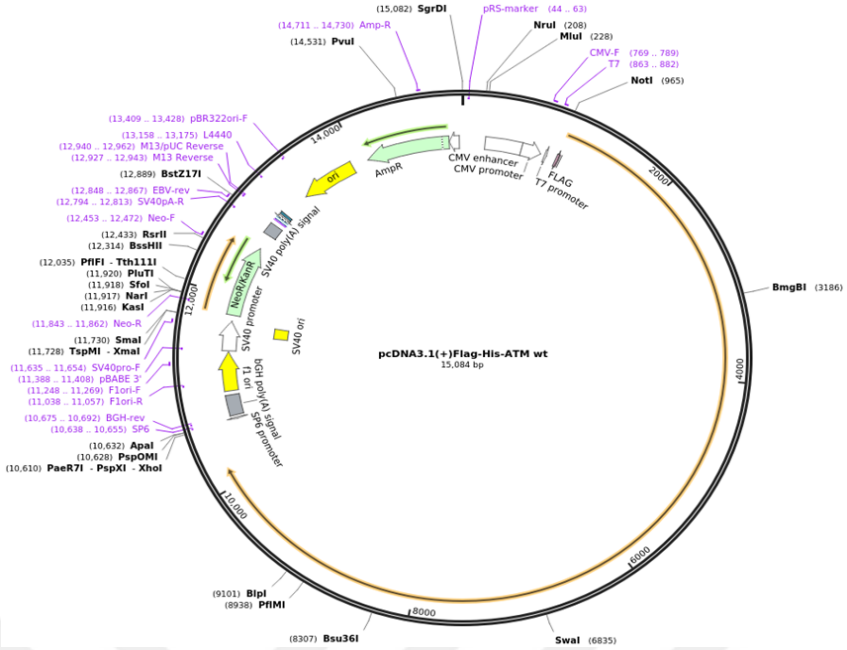

Figure 1 Full Sequence Map for "pcDNA3.1(+)Flag-His-ATM-wt" (93).

The pcDNA3.1 (+) Flag-His-ATM plasmid was purified from the liquid culture with a plasmid DNA isolation kit in accordance with the guidelines provided by the manufacturer. The nanodrop was used to measure the extracted plasmid DNA.

Verification of the plasmid DNA integrity was controlled by cutting the DNA with the SmaI, BamHI, and BamHI/HindIII restriction enzymes. After running 1 % agarose gel at 100 Volt for 1 hour, the expected bands were observed with ethidium bromide.

3.3.6.2 Primer design

We designed the in-vitro mutagenesis primers using web pages of Agilent and PrimerX (94, 95) (Table 8).

Table 8 SDM primers

Primer direction	Sequences	GC ratio	Melting ˚C
Forward	5'-gctctcagcttgatgaggatcaaacagaggctgcaaatag-3'	48 %	67˚C
Reverse	5'-ctatttgcagcctctgtttgatcctcatcaagctgagagc-3'	48 %	68˚C

3.3.6.3 Creation of the mutation

We developed an expression system to simulate *ATM* missense variations. Using the SDM technique, we created a missense variant in the full-length *ATM* gene and controlled it by sequencing. The mutant *ATM* vector was transfected into an A-T damaged cell line (GM05849). *ATM* wt cDNA was used as a positive control, and an empty vector containing no gene was used as a negative control. Additionally, expression levels were compared using a healthy cell line (GM00637).

3.3.6.4 Site directed mutagenesis

SDM primers were designed for the selected *ATM* variants and inserted into the pcDNA3.1(+)Flag-His-ATM gene with SDM technique following the QuikChange II XL Site-Directed Mutagenesis Kit protocol. Briefly, once two oligonucleotide primer sequences carrying the desired mutation were determined, primers were ordered (Sentebiolab Biotechnology, Türkiye). A PCR reaction was performed using pcDNA3.1(+) Flag-His-ATM wt, pfuUltra HF DNA polymerase enzyme, kit PCR mix, and primers carrying the desired mutation (Table 9). A control reaction was also prepared with the kit products (Table 10). As shown in Table 11 PCR cycling parameter were used to run PCR.

Table 9 PCR sample reaction mix

Sample reaction tube	Quantity
10X reaction buffer	5 µl
dsDNA template (ATM)	5 µl (50 ng)
Forward primer	1,25 µl (125 ng)
Reverse primer	1,25 µl (125 ng)
dNTP mix	1 µl
QuikSolution	3 µl
ddH2O	33,5 µl (final volume 50 µl)
PfuUltra HF DNA polymerase	1 µl

Table 10 PCR control reaction mix

Control reaction tube	Quantity
10X reaction buffer	5 µl
pWhitescript 4.5-kb control plasmid	2 µl (10 ng)
Forward primer	1,25 µl (125 ng)
Reverse primer	1,25 µl (125 ng)
dNTP mix	1 µl
QuikSolution	3 µl
ddH2O	36,5 µl (final volume 50 µl)
PfuUltra HF DNA polymerase	1 µl

Table 11 PCR cycling parameters

Reaction segment	Cycles	Temperature	Sample reaction	Control reaction
Initial denaturation	1	95˚C	1 min	1 min
Denaturation	18	95˚C	50 sec	50 sec
Annealing		60˚C	50 sec	50 sec
Extension		68˚C	15 min	5 min
Final extension	1	68˚C	7 min	7 min

Each amplification reaction was treated with Dpn1 endonuclease to remove the parental DNA template at 37˚C ON.

3.3.6.5 Transformation assay

The control and sample reactions were transformed into XL10 Gold ultracompetent cells according to the SDM kit and Addgene ATM plasmid transformation protocol (96).

Briefly, for each reaction, 45 µl ultracompetent cells were aliquoted to pre-chilled 14 mL polypropylene round-bottom tubes, and 2 µl of the β-mercaptoethanol added to it and incubated on ice for 10 min. To the tubes, 2 µl of the Dpn I treated control and sample DNA were added and incubated for 30 min on ice, then incubated

for 42 sec at 42°C water bath and then 2 min on ice, respectively, mixed with 500 µl of sterile NZY^+ broth, and put on a 37°C shaker for 1 hour at 230 rpm. Transformation reaction plated onto LB Agar Ampicillin (100 µg/mL) plates incubated at 30°C for 48 hours. Likewise, to test the transformation efficiency, vectors containing pWhitescript mutation control and pUC18 transformation control were plated onto the LB Agar Ampicillin plates containing 5-bromo-4-chloro-3-indolyl-β-D-galactopyranoside (X-gal) and 20 mM isopropyl-1-thio-β-D-galactopyranoside (IPTG). The colonies formed on the agar plate were inoculated into 2X LB broth with Ampicillin at 30°C for up to 2 nights at 250 rpm. Then, the DNA was isolated from the culture using the maxiprep plasmid isolation kit according to the protocol. Isolated DNA quantification was measured with nanodrop. The DNA was amplified with designed PCR primers before Sanger sequencing.

Mutagenesis control primers were designed with NCBI primer blast and controlled with primer design web pages: oligo analyzer, SNPCheck, and USCS in silico. Gradient PCR was performed with the designed primers (Table 12). We ran it on a 2 % agarose gel and visualized it with ethidium bromide.

Table 12 Gradient PCR primers

Primer direction	Sequences	GC ratio	Melting ˚C
Forward	5'-ccagaggtagccagaagaagc-3'	57,14 %	60,13˚C
Reverse	5'-gtgcctcaacacttctgacc-3'	55,00 %	58,77˚C

It was proven that the mutation was carried out by following the protocol of the BigDye™ Terminator V3.1 Cycle Sequencing Kit (Thermo Fisher Scientific, USA) and Sanger sequencing using the ABI 3130 Genetic Analyzer device (Thermo Fisher Scientific, USA) to check whether it carried the desired mutation using the DNA sequencing (Sanger sequencing) method.

3.3.6.6 Transfection assays

Cell growth medium was prepared by mixing DMEM with 4.5g/L D-glucose, L-glutamine, and Pyruvate (Gibco), 10 % FBS, and 1% Penicillin/Streptomycin.

Immortalized fibroblast cells without ATM protein (GM05849) and, as a positive control, immortalized fibroblast cells with ATM protein (GM00637) were obtained from the Coriell Cell Institute (97). Expression vector pcDNA3.1(+) Flag-His-ATM containing mutant and wt genes and as a negative control empty plasmid pcDNA3.1/His C (Invitrogen, USA) was transfected into GM05849 cells using FuGENE® HD Transfection Reagent (Promega, USA) according to the kit protocol. For transfected cell selection, Geneticin was added to the transfection medium at different time points.

After transfection, cells were harvested at different time points in the presence of a radiomimetic agent, bleomycin or not. The desired number of cells was washed with ice-cold PBS and centrifuged for 5 min at a maximum speed of 4˚C in a microcentrifuge. The supernatant was removed, and the pellets of the samples were frozen in liquid nitrogen. All transfection procedures were performed in duplicate.

3.3.6.7 RNA quantification

RNA extraction was performed according to the RNeasy Plus Mini Kit (Qiagen, The Netherlands) procedure. Isolated RNAs were synthesized as cDNA using RevertAid First strand cDNA synthesis kit (ThermoScientific). Then, *ATM* gene expression values were analyzed on the BioRad GFX device (Bio-Rad in, USA) accordance with the SYBR-Green PCR Master Mix (Life Technologies) according to kit procedure. In addition, GAPDH gene expression values were used as an internal control, and the results were normalized according to these values. Relative alterations in expressed genes ascertained from real-time quantitative PCR were computed using the 2-ΔΔCT technique. The Ct value of *ATM* expression was analyzed by subtracting the Ct value of the internal control GAPDH. The study was

carried out in 2 repetitions. *ATM* expression amounts in the GM00637 healthy cell line, *ATM* wt transfected into the GM05849 A-T damaged cell line, *ATM* containing the variant, and empty vector experimental groups were compared by RT-PCR method in the presence and absence of bleomycin.

3.3.7 Experimental methods of the second project

3.3.7.1 PBMC isolation

Venous blood samples were collected into 10-mL EDTA tubes. PBMCs were separated from whole blood according to the manufacturer's instructions, with some modifications, using a Ficoll-Paque PLUS density gradient solution.

The study participants' blood was mixed with an equal volume of phosphate-buffered saline (PBS) buffer and then layered slowly on top of the density gradient solution. After 400 g, 20 min, and 9/0 centrifugation, PBMCs were collected from the layer between the Ficoll and the blood plasma. Collected PBMC was washed with three volumes of PBS and centrifuged at 200 g, 10 min, and 9/9. The supernatant was discarded, the cell pellet was resuspended in 1 mL advanced RPMI 1640 medium with 10 % FBS, and then cells were counted with cell counting slides.

3.3.7.2 Comet assays

Single-cell gel electrophoresis were done with Comet assay kit in accordance with the guidelines provided by the manufacturer. We made some modifications to these protocols. Briefly, $1x10^6$ PBMCs were treated with 0.5 μM doxorubicin in the RPMI, 10 % FBS solution for 1 h at 37˚C in the dark. The treated and untreated samples were centrifuged at 100 g, 10 min RT, and the pellet was washed with ice-cold Dulbecco’s PBS. PBMCs mixed with 0,5 % low melting point agarose in a 1:10 ratio and layered onto comet slides. After incubation at 4˚C for one hour in darkness, the slides were moved to a lysis solution cooled with DMSO and left at 4˚C for an overnight period. Following the lysis, slides were submerged for one hour at 4˚C in darkness in a newly made alkaline unwinding solution. The electrophoresis has been

performed for 40 minutes in darkness at 20 V and 4˚C. The slides underwent three 5-minute washes, two with distilled water and one with 70 % ethanol. Drops were drained at 37˚C for 20 min in the dark. The circles on the slides were stained with 100 µl SYBR gold solution for 30 min in the dark and then washed with dH2O.

Slides were analyzed using the Vert.A1 fluorescence microscope used with x10 magnifier, and then the ZEN program was used to take pictures. Cells were counted randomly. The CometScore 2.0.0.38 TriTek software was used to score the obtained cell pictures (98). We analyzed the data by considering DNA proportion in the comet's "tail" as mentioned in the review of statistical comet analysis methods [15]. We compared 100 cells per slide and two slides per person. We excluded hedgehog cells to calculate the DNA percentage ranges in untreated and treated cells. Two single-blind researchers counted the slides.

3.3.8 Preparation of protein lysates

According to the cell number, cell pellet mixed with radioimmunoprecipitation (RIPA) buffer and kept 30 min on ice. Each sample was sonicated on ice, at a frequency of 20KHz, 20 pulses, 2X10 seconds, and put on ice for 5 min. Then tubes were centrifuged for 15 min at maximum speed at 4˚C in a microcentrifuge. The supernatant was taken as much as possible and then placed in a new labeled tube. Lysate was stored at -80 ˚C. The protein amount was determined using the Bradford protein assay, with BSA as a reference. In accordance with measurements and calculations, the required amount of sample buffer (5X Laemmli) was added to the lysates to reduce and denature the samples for 5 min at 95˚C.

3.3.9 Protein separation

Every phase of the SDS-PAGE assay was validated because of the biggest and smallest molecular weights of the proteins studied in these assays. We wanted to see ATM (350kD) and γH2AX (15kD) protein bands in the same gel and membrane. For that reason, we prepared our in-house tris-glycine gels, whose polyacrylamide

concentrations varied 4 %, 6 %, 10 %, and 15 %. Samples and the marker were loaded into wells, and proteins were separated at 80 V 80 min, then 100 V 120 min.

Table 13 Preparation of separating gel

Separating gel concentration	15 %	10 %	6 %
ddH2O	0,5 ml	0,8 ml	1,1 ml
30 % Acylamide/Bis	1 ml	0,67 ml	0,4 ml
1,5 M Tris pH 8,8	0,5 ml	0,5 ml	0,5 ml
10 % SDS	20 µl	20 µl	20 µl
10 % APS	20 µl	20 µl	20 µl
TEMED	2 µl	2 µl	2 µl

Table 14 Preparation of stacking gel

Stacking gel concentration	4 %
ddH2O	1,5 ml
30 % Acylamide/Bis	0,335 ml
0,5 M Tris pH 6,8	0,625 ml
10 % SDS	25 µl
10 % APS	25 µl
TEMED	2.5 µl

3.3.10 Western blotting

SDS-PAGE used for protein separation and the gel transferred to the transfer buffer for equilibration. PVDF membrane was activated with methanol for 2 min, washed with water 30 seconds, and equilibrated in 1X transfer buffer for 10 min. Also two pieces of absorbent filter papers and the sponges soaked in the transfer buffer at the same time. The transfer sandwich module was constructed and fitted to the transfer cassette. The transfer continued with pre-chilled transfer buffer (for high molecular weight proteins) for 2 hours at 50 V on the ice.

After transfer, PVDF membranes blocked in 5 % milk powder or 5 % BSA blocking (phosphorylated proteins) buffers for 1 h at room temperature. Primary antibody incubation was performed overnight at 4°C with phospho-Histone-H2AX, ATM, chek2, p53 and phosphorylated form of ATM, chek2, p53 and β-Actin. Next day after washing steps secondary antibody incubation was performed with anti-mouse IgG HRP-linked and anti-rabbit IgG HRP-linked antibodies for 1 h at room temperature. Membranes imaged using an electrochemiluminescence (BIO-RAD ChemiDoc™ MP Imaging System) system with Pierce™ ECL Plus Western-Blotting Substrate (Thermo Fisher, USA) or SuperSignal™ West Femto Maximum Sensitivity Substrate (Thermo Fisher, USA). Under identical circumstances, every experimental sample and control set was performed on separate gels or blots. Every sample was examined separately at least three times. Normalization of the relative protein levels was done using β-actin.

3.3.11 Statistical analysis

All graphical representations were plotted using the GraphPad Prism 9 software. Statistics were evaluated with the same program, taking the pooled samples into account. For the comet, western blot, and PCR assays, the Anderson-Darling, D'Agostiono, Shapiro-Wilk, and Kolmogorov-Smirnov normality tests were run to see if the participants had a Gaussian distribution. Paired t-test was applied to compare subjects before and after drug induction. Welch's ANOVA test was performed to compare the different groups of subjects. $P<0,05$ indicated a statistically significant difference; results $p\leq0,05$ were considered statistically significant (GraphPad InStat). Comet assay data were presented as the means of % tail DNA ± standard deviation of the mean.

4 RESULTS

4.1 Reported Variants ClinVar Classification

In conjunction with our collaborating hospitals and laboratories, we have recently undertaken a retrospective evaluation of the results of the hereditary cancer panel. Our primary focus was to reclassify the VUSs by scrutinizing the outcomes of individuals with a history of HBOC.

We found 1166 variants in the reports of 1200 patients whose gene panel was studied with the NGS method due to hereditary cancer predisposition, presented in Figure 2. Then, we classified these variants according to the ClinVar database and detected 281 B/LB, 130 P/LP, and 590 variants of unknown clinical significance (VUS—261 / conflicted—329) (Figure 3), and 165 were also not reported in the database.

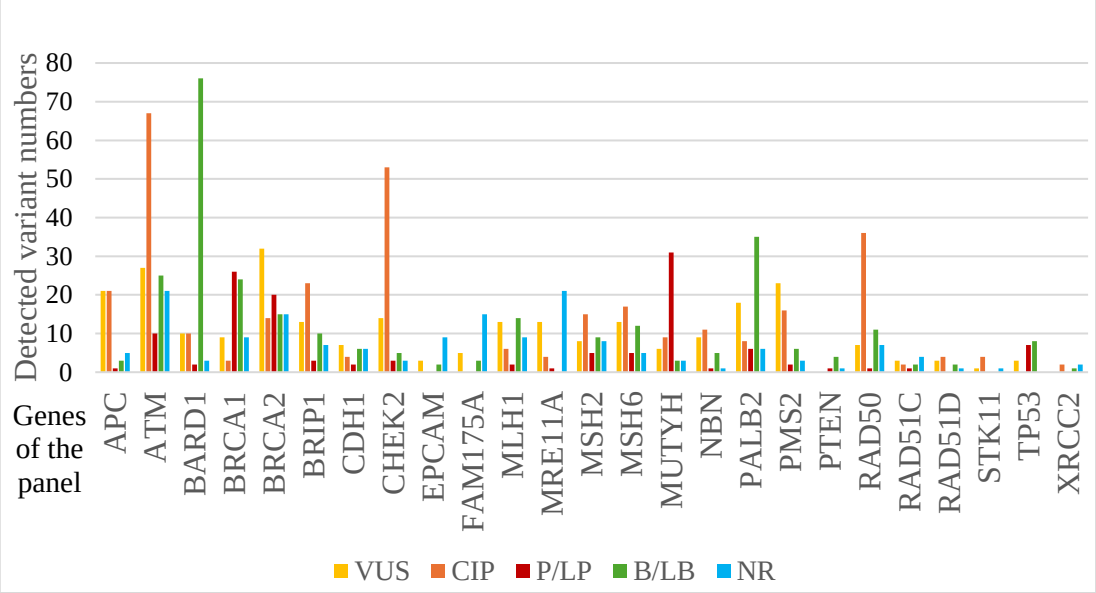

Figure 2 ClinVar classification for the HBOC panel reports. Clinical consequences were grouped according to Benign/Likely benign (B/LB), Variant of uncertain significance (VUS), pathogenic/likely pathogenic (P/LP), conflicting interpretations of pathogenicity (CIP), and not-reported (NR).

According to the data obtained, we started the first project with the *ATM* gene, which has the highest number of unknown variants, and then continued to the second project with the *BRCA2* gene variants.

In the first project, we detected 115 variants of unknown clinical significance (27 VUS / 67 CIP/ 21 NR) in the *ATM* gene (Figure 3). In the second project, 89 distinct BRCA2 variations were identified from 107 individuals (Figure 3), of which 46 represent CIP/ VUS and 15 represent NR.

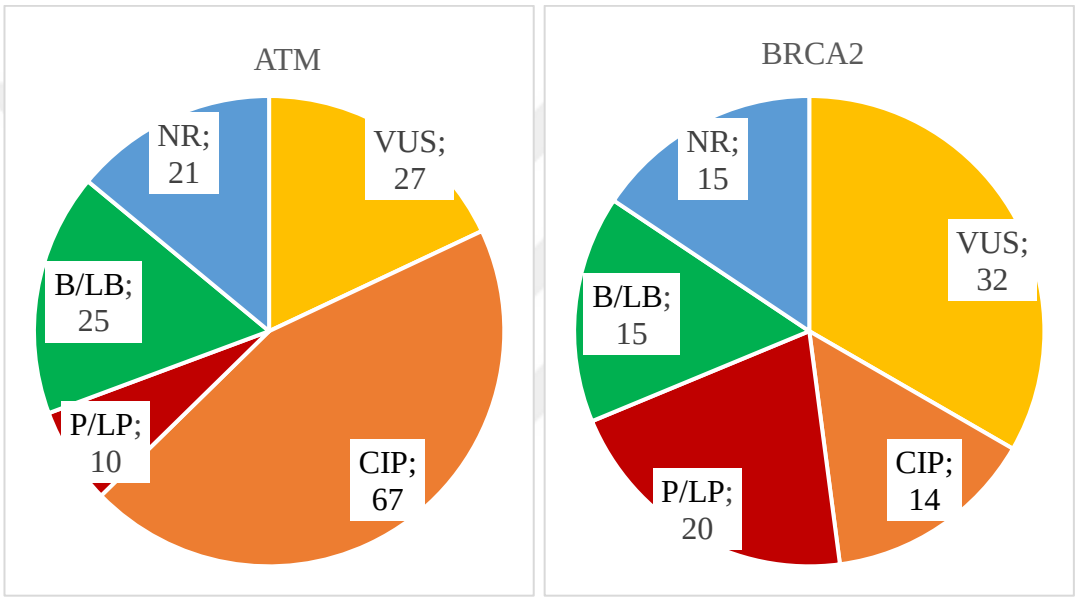

Figure 3 ClinVar classification of the variants

In these projects, we wanted to establish functional studies for *ATM* and *BRCA2* SNV missense VUS and filtered the cohort. We found 60 *ATM* and 41 *BRCA2* missense SNVs in the cohort.

4.2 Results of the ATM Project

4.2.1 Computational results of the ATM variant

After filtering the *ATM* variants, we collected their computational results and chose the five variants prone to pathogenicity. We also collected the clinical information of these five variant carriers, and some were excluded from the study. With the evaluations made with other in silico prediction tools mentioned in the method section and later added to the literature, as well as in dbNSFP, and the addition of the clinical stories of the patients to our results, the variant c.7793G>A, p.(Arg2598Gln) was selected most prone to pathogenicity among all variants.

Each in silico prediction tool has its own scoring system. To make comparisons between each other, the rank score values of all the scores we used were included in the study, and with the standard comparison method, results close to 1 were evaluated as a criterion of susceptibility to pathogenicity. When measuring the pathogenicity susceptibility of the variants in our patient cohort, the average of all rankscores was taken. The most important scores are listed in Table 15.

Table 15 In silico annotation of the selected variant

Selected variant and in-silico databases	Results
General information	SNV ATM (NM_000051.4): c.7793G>A (p.Arg2598Gln)
Protein variation	R2598Q
Uniprot ID	Q13315
ClinVar variation ID	229826
Genome location	11:108203493
Type	SNV
MANE	ENST00000675843.1
dbSNP	rs140263969
Exon/Intron	Exon 53 in 63
ClinVar	VUS
CADD	32

Table 15 In silico annotation of the selected variant (continues)

SIFT	0,5748; damaging
SIFT4G	0,5664; damaging
PolyPhen-2	0876; probably damaging
MutationTaster	Disease causing
Mutation assessor	0,8643; moderate
M-CAP	0,9026; damaging
MVP	0,9666
MetaRNN	0,8752; damaging
BayesDel addAF	0,7193; damaging
BayesDEl noAF	0,8318; damaging
DANN	0,9994
EIGEN	0,8672
EVE	0,8424
FATHMM	0,8442; damaging
FATHMM-MKL	0,991; damaging
LRT	0,8433; damaging
REVEL	0,9072; supporting pathogenicity
PROVEAN	0,5954; damaging
PIVOTAL	0,961; highly pathogenic
UMD-Predictor	75; pathogenic

The effect of the change in protein structure as a result of variant formation was modeled with the Missense 3D-DB protein modeling programs (99). 2598R>Q; Since the deterioration in the stable structure of the protein as a result of the Arginine → Glutamine mutation will create a change in the cavity; its effect is again evaluated as damaging.

Table 16 Missense 3D protein modeling

Uniprot position	Residue wildtype	Residue mutant	Structure	Missense3D prediction	Structural damage predicted	ClinVar annotation	Change in protein-free energy (kcal/mol)
2598	ARG	LEU	5np1_A	Neutral	None	VUS	0,13
2598	ARG	GLN	5np1_A	Damaging	Cavity altered	VUS	0,14
2598	ARG	GLY	5np1_A	Neutral	None	-	0,49

4.2.2 Mutagenesis experiments results

4.2.2.1 Provement of the integrity of the plasmid

The plasmid containing the entire *ATM* gene was isolated, and its concentration was measured using a nanodrop device (Table 18).

Table 17 NanoDrop results

# of measurement	ng/µl	$A_{260/280}$	$A_{260/230}$
# 1	1012,7	1,87	2,38
# 2	1022,6	1,86	2,36

DNA integrity was checked by cutting the isolated DNA from the plasmid with SmaI, BamHI, and BamHI/HindIII restriction enzymes. Whole plasmid is 15084 bp; SmaI: 1 band at 12 kb; cut at 11,730 bp, BamHI: 3 bands at 6,4, 4,3, 4,2 kb; cut at 907 bp, 5,144 bp, 9,548 bp, BamHI/HindIII: 5,7, 3,8, 1,8, 1,6, 0,7, 0,5, 0,3, 0,2, 0,1 kb; Plasmid integrity was proven with band sizes of 3 bands BamHI cut at 907 bp, 5,144 bp, 9,548 bp / 6 bands HindIII cut at 889, 2,732, 4,368, 5,706, 9,925, 10,186 bp. The expected bands were observed, which proves that the DNA integrity is correct (Figure 4).

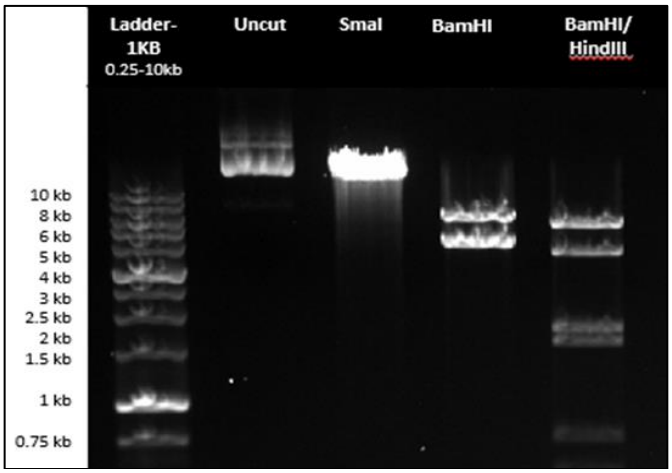

Figure 4 Plasmid restriction with enzymes. After running 1 % agarose gel an hour long at 100 V, the expected bands were observed with ethidium bromide. Whole plasmid: 15,084 bp; SmaI: at 12 kb, BamHI: at 6,4/ 4,3/ 4,2 kb, BamHI/HindIII: at 5,7/ 3,8/ 1,8/ 1,6/ 0,7/ 0,5/ 0,3/ 0,2/ 0,1 kb; Plasmid integrity was proven with band sizes.

4.2.2.2 Insertion of the mutation

The SDM PCR reaction was performed and the parental chain was removed by DpnI enzyme digestion (Figure 5).

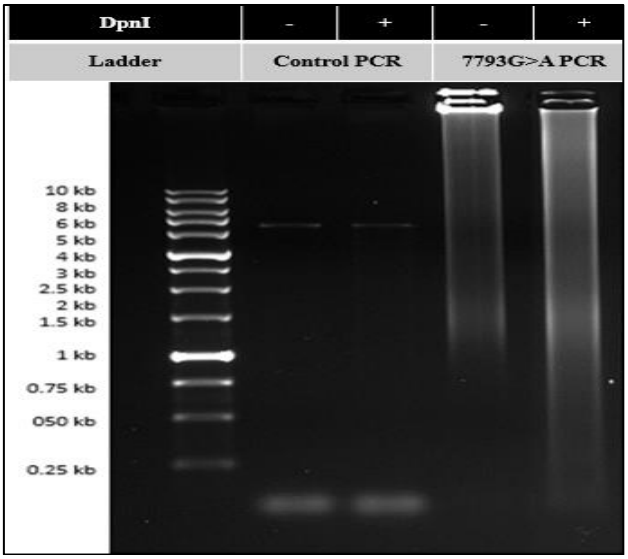

Figure 5 DpnI digestion

4.2.2.3 Transformation of the mutated plasmid

As a result of the transformation, one colony was observed on the plate where the mutation was located (Table 18). After the mutated *ATM* DNA isolation, the amount of DNA was determined with a nanodrop (Table 19).

Table 18 Transformation reaction and obtained colony numbers

Transformation Reactions	Incubation	# of colonies obtained
pWhitescript mutation control	37˚C 16 h	495
pUC18 transformation control	37˚C 16 h	48
Sample mutation	30˚C 48 h	1

Table 19 NanoDrop measurement of mutated ATM plasmid isolation

# of measurement	ng/µl	$A_{260/280}$	$A_{260/230}$
# 1	1382,3	1,88	2,33
# 2	1378,2	1,88	2,36

4.2.2.4 Proven of the mutation

We performed gradient PCR at 60,9˚C, 59,4˚C, and 58,2˚C and amplified the isolated DNA with the designed PCR primer. We checked the product with the most suitable melting temperature, 60,9˚C. The mutation we created was proven by Sanger sequencing (Figure 6).

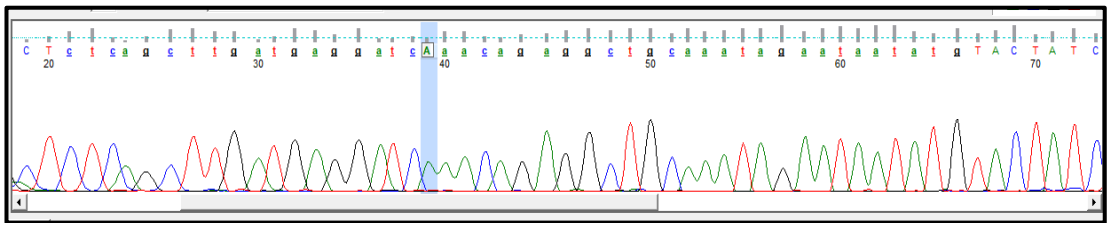

Figure 6 Sanger sequencing result

4.2.3 Functional analysis results of the ATM variant

The pcDNA3.1(+) Flag-His-ATM expression vectors containing wt and mutant *ATM* genes and the empty vector were transfected into immortalized fibroblast cells lacking ATM protein, and 48 hours later, G418 was added for extra selectivity, and 72 hours later, untreated cells were harvested (Table 20). Induction with bleomycin was carried out by inducing the cells half an hour before harvesting. Cells were counted, and 75 % were split for protein and 25 % for mRNA experiments. All experimental groups were studied in duplicate.

Table 20 Used cell types and expression vectors

Coriell Cell #	Cell type	Expression vectors
GM00637	SV40 virus-transformed apparently healthy culture	-
GM05849	Ataxia-Telangiectasia	pcDNA3.1(+) Flag-His-ATM wt
GM05849	Ataxia-Telangiectasia	pcDNA3.1(+) Flag-His-ATM mutated
GM05849	Ataxia-Telangiectasia	pcDNA3.1(+) His empty vector

4.2.3.1 Gene expression

ATM and internal control *GAPDH* mRNA expression was compared between experimental groups: the GM00637 healthy cell line, *ATM* wt, *ATM* containing the variant, and empty-vector after transfected into the GM05849 A-T damaged cell line.

As expected, *ATM* expression was at the lowest level in the negative control group, which did not contain the *ATM* gene. As shown in the figure 7, expression levels increased in the experimental groups compared to the negative control. Gene expression levels were approximately the same between the healthy and *ATM* wt carrier-deficient cell lines. Besides *ATM* mutated variant carrier deficient cell line expressed 3-fold more *ATM* than these cell lines ($p<0,0001$). In addition, after ble-induction, *ATM* expression increased in the cell lines.

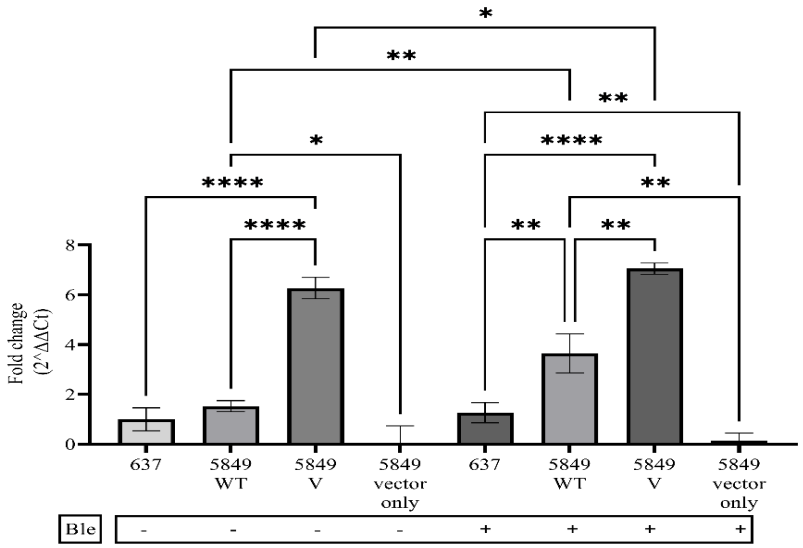

Figure 7 ATM gene expression. To compute the relative changes in gene expression derived from real-time quantitative PCR studies, the 2-ΔΔCT technique was employed. GAPDH (internal control). 637 healthy cell line, ATM wt transfected into the 5849 A-T damaged cell line, ATM containing the variant 5849-V, and empty vector experimental groups were compared by RT-PCR method in the presence and absence of bleomycin (ble). The average ± SD of two separate, identical trials is shown in each column. (* < 0,05, ** < 0,01, *** < 0,001).

4.2.3.2 Determining the protein levels in ATM cells

In the ATM project, we induced DNA damage in the experimental groups using bleomycin and observed the phosphorylation levels of the expected substrates in the DNA damage pathway. To determine the pathogenicity of the *ATM* variant, we examined its effects on ATM, ATM autophosphorylation, chk2, p53, and the phosphorylation of chk2 and p53 using SDS-PAGE and western blotting. We also added the histone protein H2AX, a key player in the DNA repair mechanism, to our study and observed the differences between the groups (Figure 8-11).

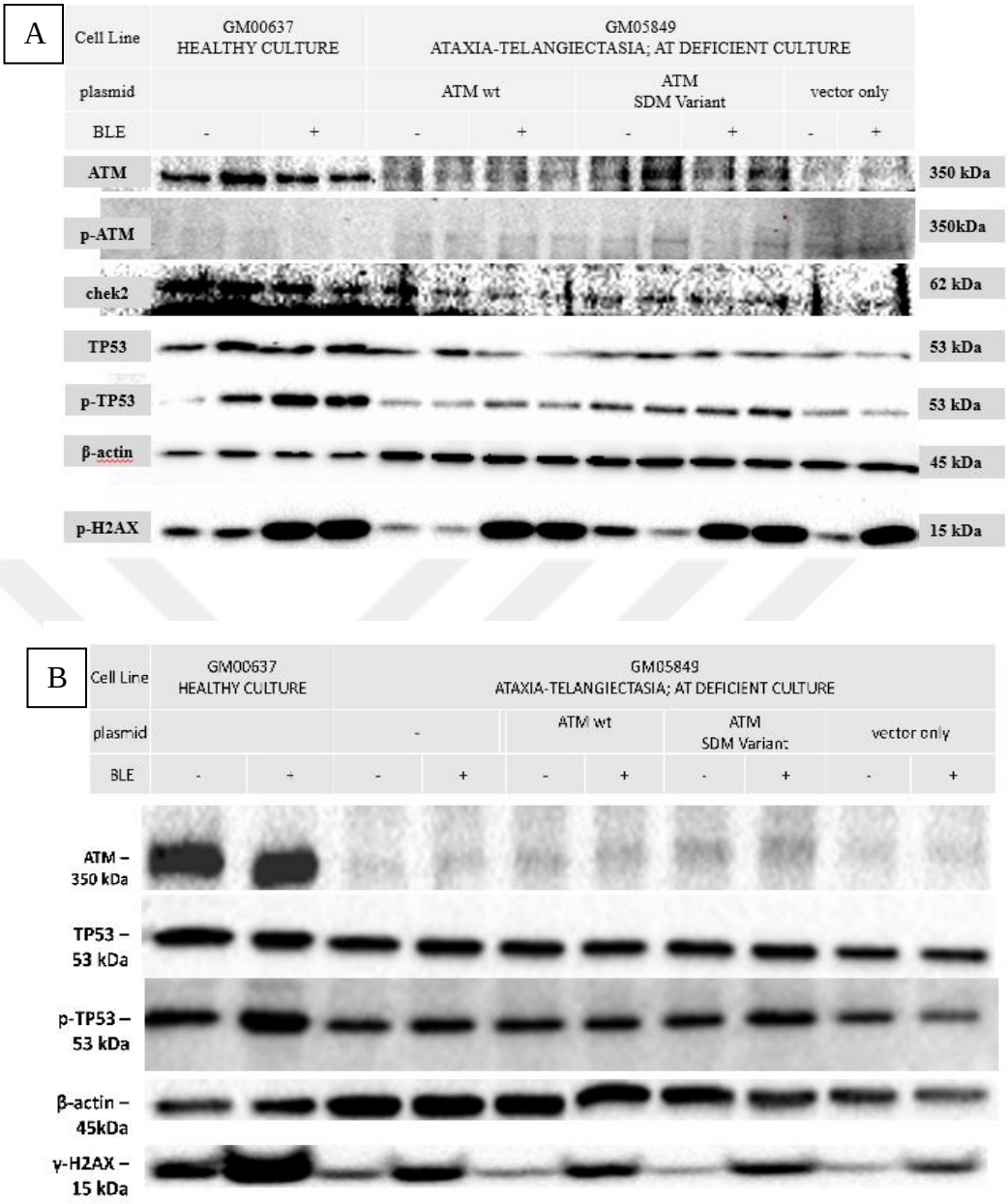

Figure 8 A and B Representative presentation of western-blot results. Band appearances of ATM, chek2, TP53, p-TP53, p-H2AX, and internal control b-actin bands obtained with proteins in cell lysates obtained after double repeat transfection. Proteins were run on 4 %-6 %-10 %-15 % SDS-PAGE at 80V for 80 minutes and 100V for 40 minutes and then transferred to the PVDF membrane. All experiments were performed in duplicate. The GM00637 is a healthy cell line, ATM wt, ATM containing the SDM variant, and empty-vector transfected into the GM05849 A-T damaged cell line. BLE: Bleomycin.

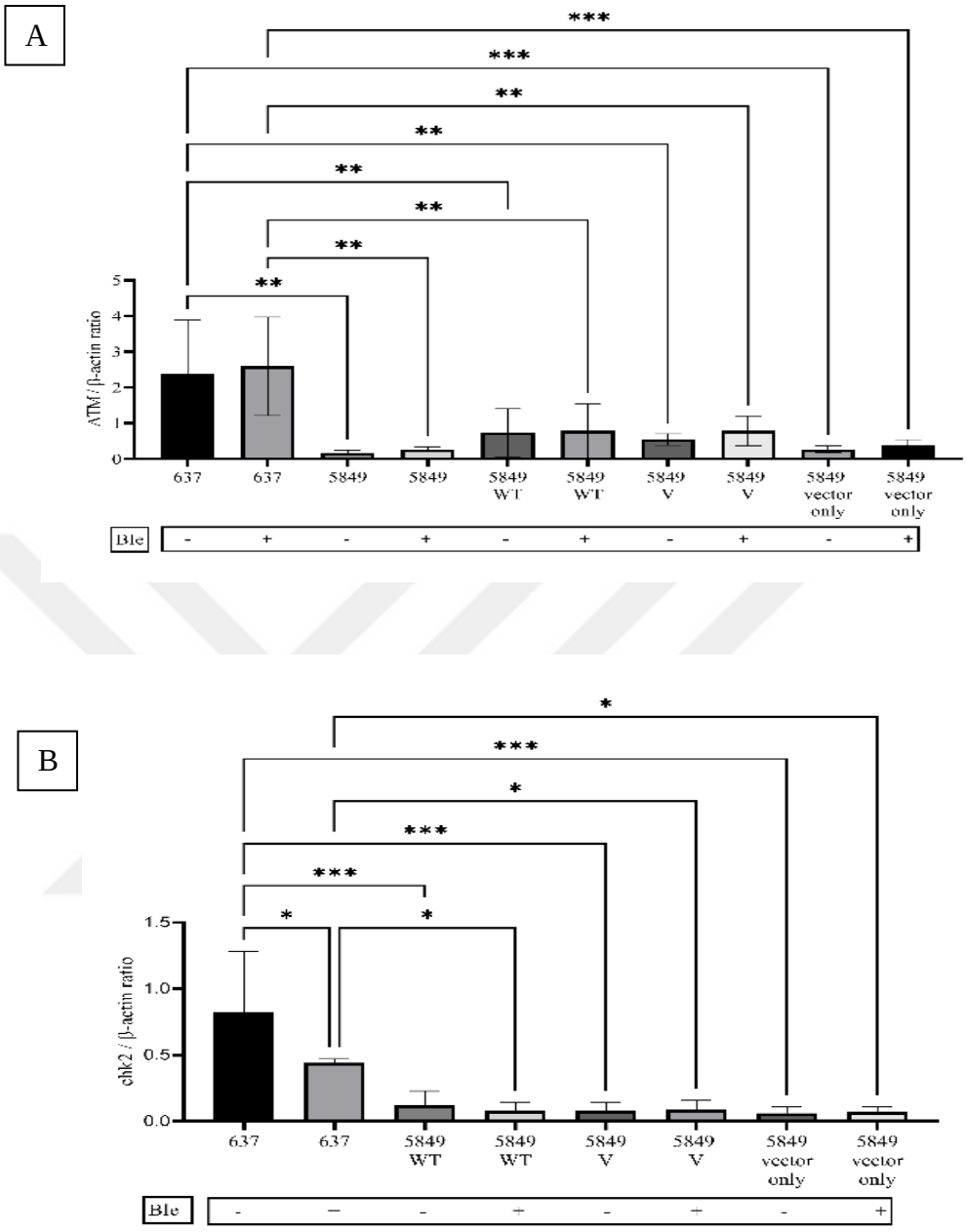

Figure 9 The quantitative western blot graph displaying the amounts of protein pre and post exposure to 1 μM 0,5 h Ble between experimental groups. (A) ATM, (B) chk2. Relative protein levels were adjusted using β-actin. Ble: bleomycin, 637: GM00637 healthy cell line, 5849: GM05849 A-T damaged cell line, 5849 wt: ATM wt in GM05849, 5849 V: ATM containing the SDM variant in GM05849, and 5849 empty-vector: empty vector transfected into the GM05849 A-T damaged cell line**.** Error bars display the standard deviation. ($\alpha = 0,05$), (* $< 0,05$, ** $< 0,01$, *** $< 0,001$).

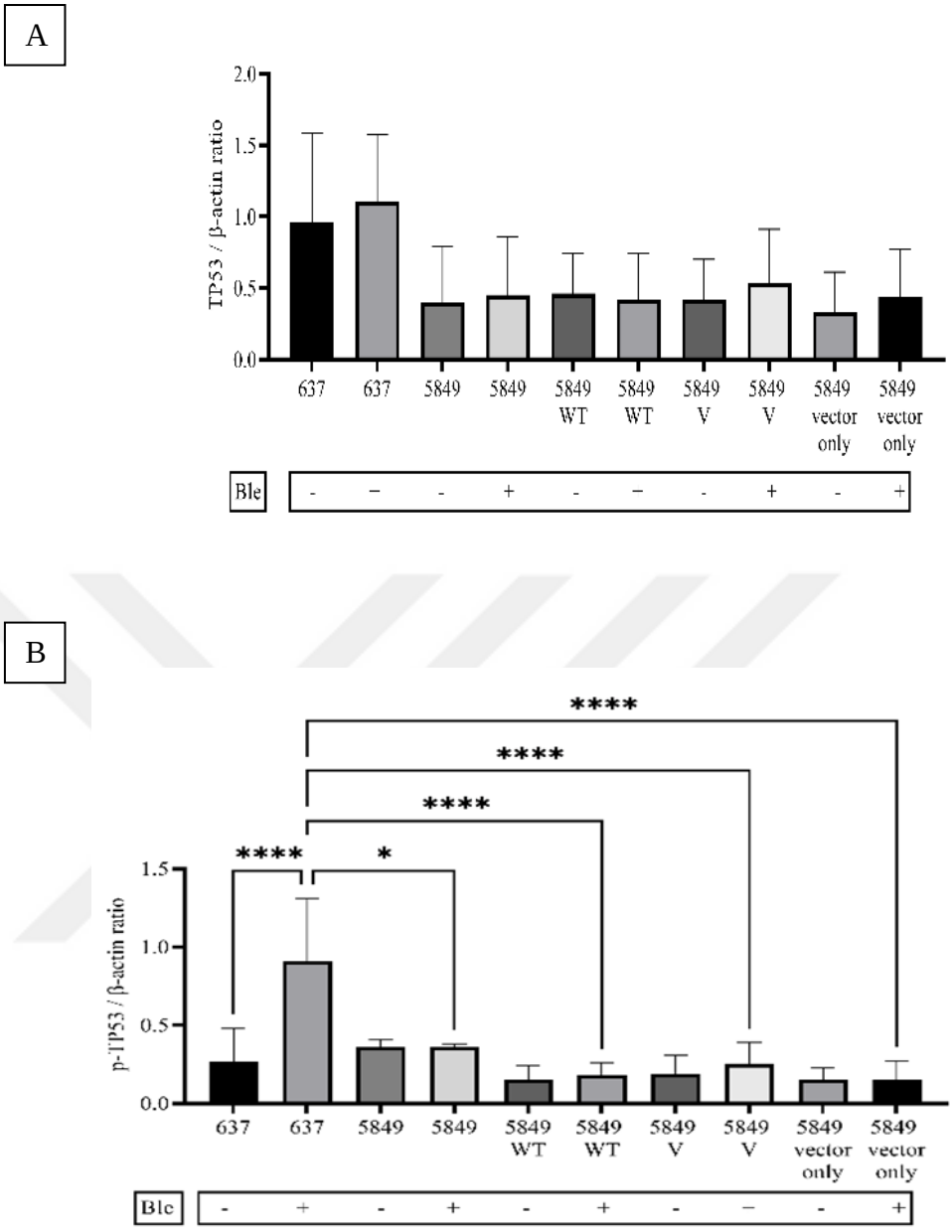

Figure 10 The quantitative western blot graph displaying the amounts of protein pre and post exposure to 1 μM 0,5 h Ble between experimental groups. (A) TP53, (B) p-TP53. Relative protein levels were adjusted using β-actin. Ble: bleomycin, 637: GM00637 healthy cell line, 5849: GM05849 A-T damaged cell line, 5849 wt: ATM wt in GM05849, 5849 V: ATM containing the SDM variant in GM05849, and 5849 empty-vector: empty vector transfected into the GM05849 A-T damaged cell line**.** Error bars display the standard deviation. ($\alpha = 0,05$), (* $< 0,05$, ** $< 0,01$, *** $< 0,001$).

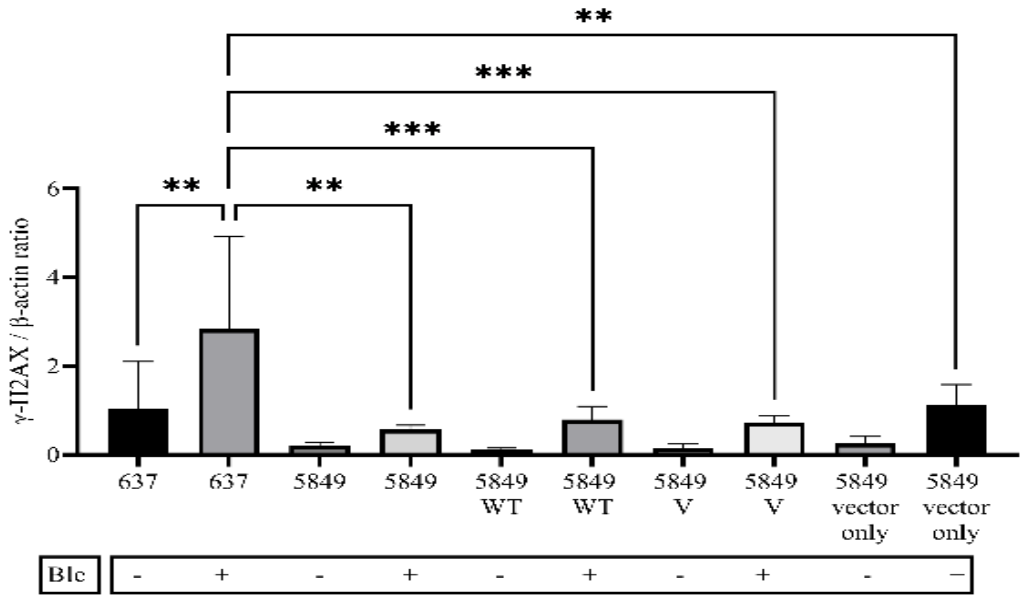

Figure 11 The quantitative western blot graph displaying the amounts of protein pre and post exposure to 1 μM 0,5 h Ble between experimental groups.
Relative protein levels were adjusted using β-actin. Ble: bleomycin, 637: GM00637 healthy cell line, 5849: GM05849 A-T damaged cell line, 5849 wt: ATM wt in GM05849, 5849 V: ATM containing the SDM variant in GM05849, and 5849 empty-vector: empty vector transfected into the GM05849 A-T damaged cell line**.** Error bars display the standard deviation. ($\alpha = 0,05$), (* $< 0,05$, ** $< 0,01$, *** $< 0,001$).

A comparison of the experimental groups revealed significant differences. Unfortunately, the expected bands in phosphorylated ATM and phosphorylated chk2 were not observed, presenting an unexpected challenge. As anticipated, the H2AX phosphorylation rate increased in bleomycin-induced cells. We did not observe any significant differences between deficient cell lines GM05849 with different expression groups on the other proteins.

The healthy cell group GM00637 exhibited the highest protein expression among all groups. After ble-induction, expression levels were as follows in GM00637: showed the same ATM, decreased chk2 ($p < 0,05$), the same TP53, 3-fold increased p-TP53 ($p < 0,001$), and 2-fold increased H2AX phosphorylation ($p < 0,01$).

4.3 Results of the BRCA2 Project

In the *BRCA2* cohort, there were 51 variants of unknown clinical significance (VUS/CIP/NR), 41 of which were identified as missense SNVs. Medical data from 45 individuals with these 41 variations were gathered from our partner hospitals in order to further the study.

Five VUS-carrier individuals with a diagnosis of BC were chosen, and their missense "*BRCA2*, NM_000059.4, NP_000050.3" SNV were as follows: "T1011R", "T1104P/M1168K", "R2027K", "G2044A", "D2819V"" (Figure 12, Table 21). A pathogenic variant carrier woman with a diagnosis of BC was involved in the study to provide positive control and has three variants on different genes: *"BRCA1*, NM_007294.4, NP_009225.1", "c.2131_2132del, frameshift K711fs deletion", a "*BRCA2,* c.4277C>T, T1426I", with an "*APC,* c.3449G>C, E1317Q". A non-variant carrier two healthy control also participated as a negative control.

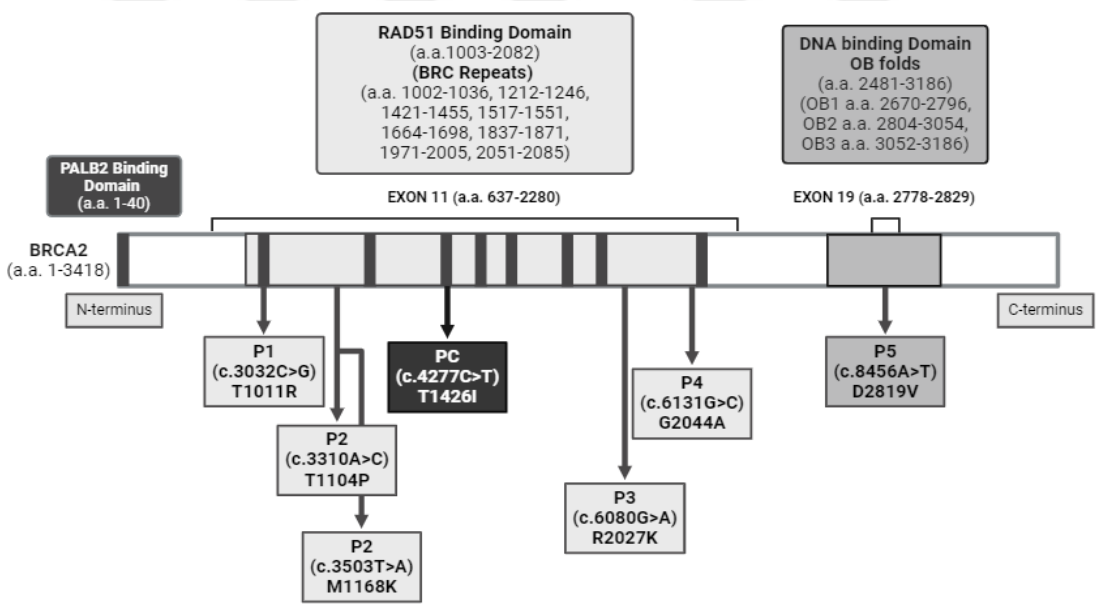

Figure 12 Chosen variants on the BRCA2 protein domains. PC: Pathogenic carrier subject, P1, P2, P3, P4, P5 VUS-carrier subjects (16).

Table 21 Selected subjects and *BRCA2* missense VUSs

Subjects	Gene	HGVS coding	Molecular Consequence	Protein Change	Exon	dbSNP	ClinVar	Prior to func. anlysis
PC	*BRCA1*	c.2131_2132 del	frameshift	K711fs	10	rs398122653	P	P
	BRCA2	c.4277C>T	missense	T1426I	11	rs748591104	CIP	
	APC	c.3949G>C	missense	E1317Q	16	rs1801166	B/LB	
P1	*BRCA2*	c.3032C>G	missense	T1011R	11	rs80358548	CIP	VUS (-)
P2	*ATM*	c.4473C>T	synonymous	F1491=	30	rs4988008	CIP	-
	BRCA2	c.3310A>C	missense	T1104P	11	rs80358577	CIP	VUS (int)
	BRCA2	c.3503T>A	missense	M1168K	11	rs80358598	CIP	VUS (-)
P3	*BRCA2*	c.6080G>A	missense	R2027K	11	rs431825337	CIP	LB
P4	*BRCA2*	c.6131G>C	missense	G2044A	11	rs56191579	CIP	LB
P5	*BRCA2*	c.8456A>T	missense	D2819V	19	rs1555287655	VUS	VUS (int)

4.3.1 Computational results of the BRCA2 variants

We evaluated the population-wide allele prevalence rates of seven variations using the gnomAD database to estimate their worldwide frequency. Our analysis unveiled that both variations in P3 and P5 had yet to be identified. In contrast, the frequencies of the other variations (PC, P1, P2, and P4) were not high in the global population. The findings suggest a moderate level of potential pathogenicity (PM2) (6). Nevertheless, the ClinGen SVI committee recommends classifying the result as B and adjusting the evidence from moderate to supporting (92, 100).

In Figure 12, it is evident that the PC, P1, P2, P3 and P4 individuals' variants are located in exon 11 in the RAD51-binding domain. This region is considered a cold spot where pathogenic missense variants are not expected. Additionally, the D2819V variant is located in the exon 19 in the DBD.

The P1 variant, identified as T1011R, is situated within the BRCA2 repeat domain. In silico prediction tools suggest that this variant will likely have a detrimental impact on the protein. Specifically, this genetic alteration results in substituting threonine (T) to arginine (R), a neutral and polar aa to a basic and polar aa.

Regarding P2 as T1104P, is highly conserved and computational analyses indicate this variant may be deleterious. Polar aa T changes to nonpolar aa proline (P) with distinctive structural properties. If P is substituted for T at position 1104, the three-dimensional form of the protein and how it interacts with different proteins or DNA might alter. However, various computational tools collectively provide B supporting evidence. Additionally, the databases show that this variation coexists with BRCA2 M1168K in seven cases. According to the study, it is the same as P2, and both are suggested to be in the "in-cis" arrangement. Concerning P2, M1168K, computational analysis tools predict this variant to be B. The BRCA2 protein may be affected functionally by the substitution of lysine (K) for methionine (M) at position 1168. Since M is a hydrophobe aa and K has a positive charge and a hydrophobe side chain. This alteration in the characteristics of aa may have an effect on the stability, form, or interactions of the protein with other molecules. P2 has also a nonsense *ATM* “NM_000051.4, NP_000042.3”, “c.4473C>T, p.Phe1491= (F149=)” variant.

For P3, R2027K, in-silico analyses indicate that the variant may not significantly impact protein function. However, replacing arginine (R) with lysine (K) at position 2027 could potentially influence the function of the BRCA2 protein. Arginine and lysine both carry a positive charge, but their side chain structures differ. This change in side chain characteristics and polarity may change the protein's structural shape or disrupt bonds between proteins.

P4, G2044A, in silico analyses suggest that the variant will not harm the protein's function. Substituting alanine for glycine (G) might or might not have a major influence on the protein's form, stability, or functionality.

Another mutation, referred to as P5 and labeled as D2819V, stated at the OB-2 region in the protein. In silico results have indicated potential detrimental effects on the protein. More precisely, replacing aspartic acid (D) to valine (V) at 2819 will probably affect the form and functionality of the protein. Additionally, V is a nonionic aa with a hydrophobe side chain, whereas D is an acidic aa with a negatively charged side chain. This change in the characteristics of aa might cause problems with protein folding, stability, and binding.

Based on the computational findings, the variations were preliminarily categorized using the ACMG/AMP "PP3/BP4" criteria prior to the functional analysis.

Table 22 In silico analysis of selected variants

Subjects	Protein Change	gnomAD	SIFT	Poly Phen	Meta RNN	DeMAG	Bayes Del addAF	Bayes Del noAF
PC	K711fs	-	-	-	-	-	-	-
	T1426I	$1,63x10^{-6}$	0,86	0,001	0,07	0,05	-0,27	-0,40
	E1317Q	-	0,02	0	0,007	0,12	-	-
P1	T1011R	$2,42x10^{-5}$	0	1	0,67	0,76	0,29	0,43
P2	F1491=	-	-	-	-	-	-	-
	T1104P	$7,62x10^{-6}$	0	1	0,65	0,64	0,06	-0,09
	M1168K	$7,53x10^{-6}$	0,16	0,006	0,30	0,08	-0,19	-0,49
P3	R2027K	-	0,49	0,009	0,11	0,06	-0,23	-0,57
P4	G2044A	$1,43x10^{-5}$	0,7	0,062	0,11	0,06	-0,31	-0,50
P5	D2819V	-	0	0,964	0,84	0,62	0,40	0,33

We assigned variants according to PP3, indicating a detrimental impact and designated, and designated P1; VUS (−), P2-T1104P; VUS (int)/ M1168K VUS (−), and P5; VUS (int). Nonetheless, based on the BP4, we concluded that P3 and P4 are LB (Table 22).

4.3.2 Functional analysis of the BRCA2 variants

4.3.2.1 Exposure to doxorubicin decreases DNA damage levels in the study participants

At the onset of the study we evaluated the average DNA damage levels of all groups together. Before and after an hour long exposure to 0,5 μM Dox, the DNA percentage in the tail remained relatively constant (21±6 vs 18±9) (Figure 13A). The H2AX phosphorylation level indicates a decrease in DNA damage levels, as evidenced by a 50 % reduction in (0,6±0,5 vs 0,3±0,2) (Figure 13 B)

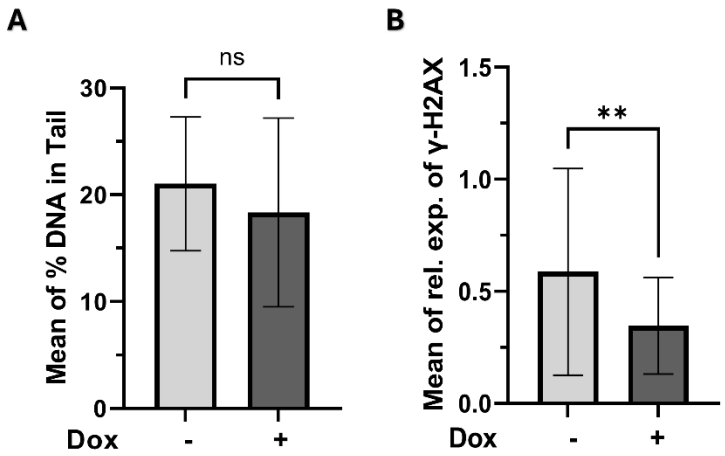

Figure 13 Subjects pre- and post- exposure to one hour long 0,5 μM dox (Dox). A: After doxorubicin induction, DNA damage decreased but was not significantly different (ns). B: λ-H2AX protein expression decreased after dox exposure (p=0,0016) Relative protein levels were adjusted using β-actin. (alpha=0,05), (** <0,01).

4.3.2.2 Healthy controls showed increased DNA damage after dox induction

The individuals were then split into groups of non-carriers (NC) and variant carriers (subjects) so that we could examine the DNA damage amounts. We investigated the impact of dox-induction on NC cells and found that an hour of 0,5 μM Dox treatment significantly increased DNA damage. The mean DNA percentage in the comet's tail increased 1,6 times in the NC group (20±3,5 to 32±2,3) (Figure 14A), but no significant effect was observed on the H2AX phosphorylation

levels (p>0,05) (Figure 14B). Increased DNA damage observed in non-pathological individuals due to the drug verifies the suitability of the dosage and duration used in our studies. On the other hand, the variant carriers group showed a decrease in damaged DNA levels after exposure to Dox, indicated by a decrease in the tail's DNA % (21,4±7 to 13,7±2) (Figure 14A) and phosphorylated H2AX levels (0,6±0,5 to 0,3±0,2) (Figure 14B).

We found no statistically significant difference in the DNA percentage in the comet tail of cells between the two groups (Figure 14A). However, the group carrying the variant showed an increase of 2,7-fold in H2AX phosphorylation levels in contrast to the NC group (0,2±0,05 vs 0,7±0,5) (Figure 14B). Following Dox exposure, the percentage of DNA in the tail of cells between NC and VC groups decreased by 0,4-fold (32±0,6 vs. 14±2,3) (Figure 14A). Interestingly, the two groups had no significant difference in the H2AX phosphorylation levels after Dox-induction (Figure 14B).

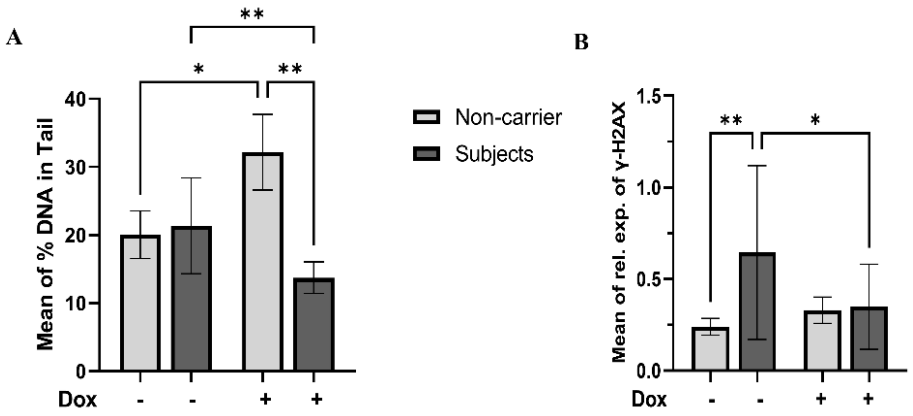

Figure 14 Comparison of non-carrier healthy controls with variant carrier subjects before (DN) and after (DP) 1 hour long exposure to 0,5μM Dox. A: After induction, the average DNA from the tail percentage increased in healthy cells and decreased in variant carriers. B: After induction healthy cells show slight increase in λH2AX with no significant difference but subjects reduced. Relative protein levels were adjusted using β-actin. (*p<0,05, **p<0,01). (alpha=0,05).

4.3.2.3 Pathogenic variant carrier showed noticeably elevated endogenous DNA damage

We determined the degree of damaged DNA by categorizing the participants into three groups: two healthy individuals with no variation one with a identified pathogenic variation, and five with VUS.

The results from the DNA content in the tail showed that the PC group had endogenous DNA damage levels 1.7 times higher than those of the NC and VUS groups, with values of 34±6,7 for the PC group, 20±3,5 for the NC group ($p > 0,05$), and 18,8±3,6 for the VUS group ($p > 0,05$) (Figure 15A). Following Dox exposure, the NCs average DNA from the tail % (32±5) increased by two and 2,5 times, respectively, relative to the PC (17±2,1,) and VUS-Cs (13±1,8) (Figure 15A). After analyzing the changes in all groups, the non-carrier negative controls displayed a 1,6-fold rise after the induction of Dox (20±3,5 to 32±5,5) (Figure 15A). The PC declined by 50 % (from 34±6,7 to 17±2,1), and the VUS-Cs declined by 70 % (from 19±3,6 to 13±1,8). (Figure 15A).

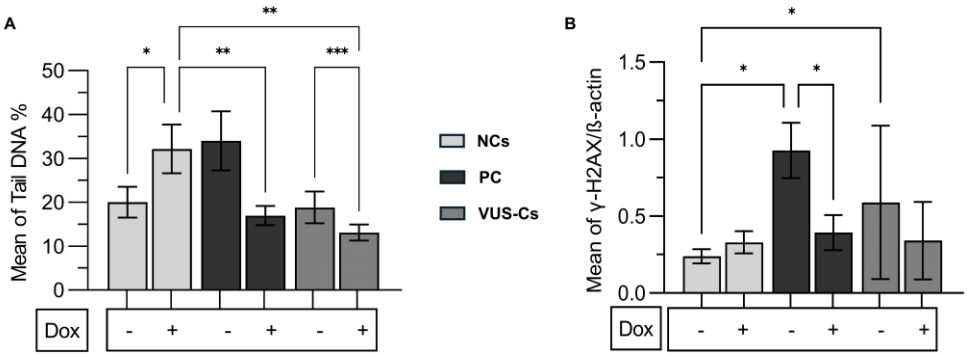

Figure 15 The average values of non-carriers (NCs), pathogenic variant carrier (PC), and VUS carrier (VUS-Cs) individuals were analyzed before and following an hour long 0,5 μM doxorubicin exposure. (A) The average DNA from the tail percentage. (B) γH2AX/ β-actin ratio. ($\alpha = 0,05$), (* < 0,05, ** < 0,01, *** < 0,001) (16).

The results of the H2AX phosphorylation showed that the PC increased 4-fold in endogenous γH2AX levels (0,9±0,2) relative to the non-carrier negative controls

(0,2±0,04). The level of PCs was 1,5 times greater than that of VUS-Cs (0,6±0,5) (Figure 15B). The VUS-Cs exhibited a level of 0,6±0,5, 2,5 times higher than that of the non-carrier negative controls (0,2±0,04). Nevertheless, after Dox exposure, no discernible change was seen among the groups (Figure 15B). When internal and external damaged DNA amounts were compared between the NCs and VUS-Cs, no statistically significant variation was seen, except for the PC, which demonstrated a 0,4-fold decline (0,9±0,2 to 0,4±0,1) (Figure 15B).

It was found that the PC had higher damaging DNA compared to the NCs. The PC variant further supports its classification as a pathogenic variation by damaging the DBD of both BRCA1 and BRCA2.

4.3.2.4 Understanding the differences between VUSs must be considered

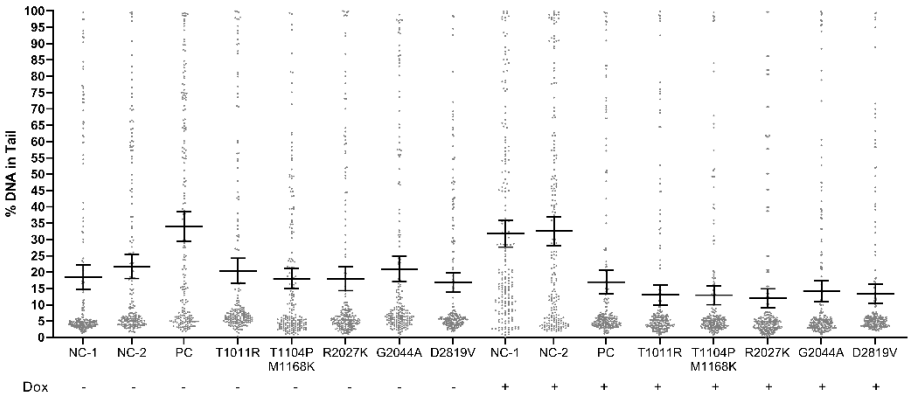

Figure 16 Percentage of DNA content of tails for every individual before and following an hour long 0,5 μM Dox exposure. Mean values with 95 % Confidence Interval. NC: Non-carrier, PC: Pathogenic carrier (16).

Figure 16 represents the DNA from the tail percentage of all subjects. Comparing NC-1 to NC-2 reveals variations in internal and external damaged DNA levels in two individuals within the healthy control group.

.

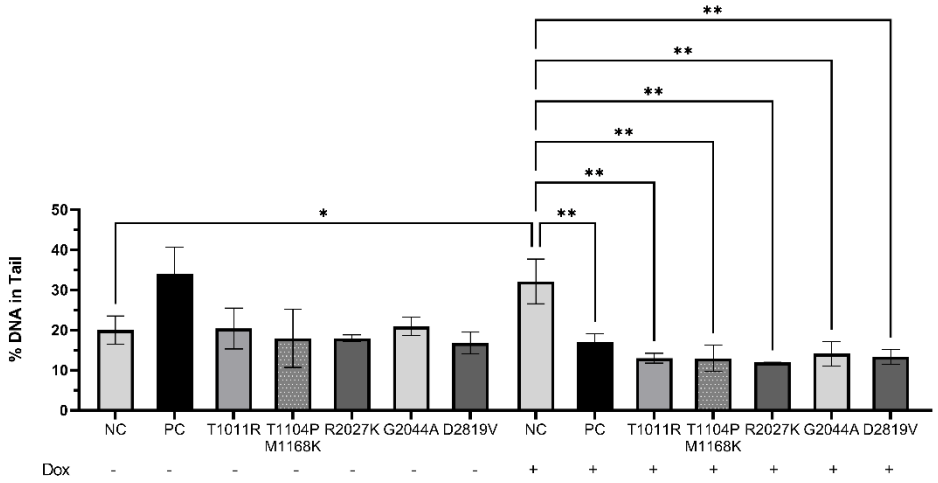

Figure 17 Comparison negative (NC) and positive (PC) controls with VUS carrier individuals prior to and following an hour long 0,5 μM Dox exposure. (α = 0,05), (*p<0,05, **p<0,01) (16).

The study revealed that the average proportion of % DNA in the tail was comparable for internal NCs (20±3,5) and VUS-Cs (20±3,6). However, the PC (33,98±6,7) doubled the amount. In contrast, following Dox exposure, the average of NCs become approximately two fold (20±3,5 to 32±5,5), while the PC reduced by a similar magnitude (34±6,7 to 17±2,2) (Figure 17). After exposure to Dox, NCs % DNA in the tail was approximately 2,5 times greater than that of VUS-Cs, as depicted in Figure 17. The % DNA in the tail of VUS-Cs reduced following Dox exposure. Specifically, P1 (T1011R) reduced 65 % from 20±5,09 to 13±1,2. Similarly, P2 (T1104P/M1168K) demonstrated a 1,4-fold decrease from 18±7,2 to 13±3,2. P3 (R2027K) showed a 1,5-fold decrease from 18±0,8 to 12±0,03. Furthermore, P4 (G2044A) displayed a 1,5-fold decrease from 21±2,2 to 14±3,02, and P5 (D2819V) experienced a 1,3-fold decrease from 17 ± 2,2 to 13 ± 1,8 (Figure 17).

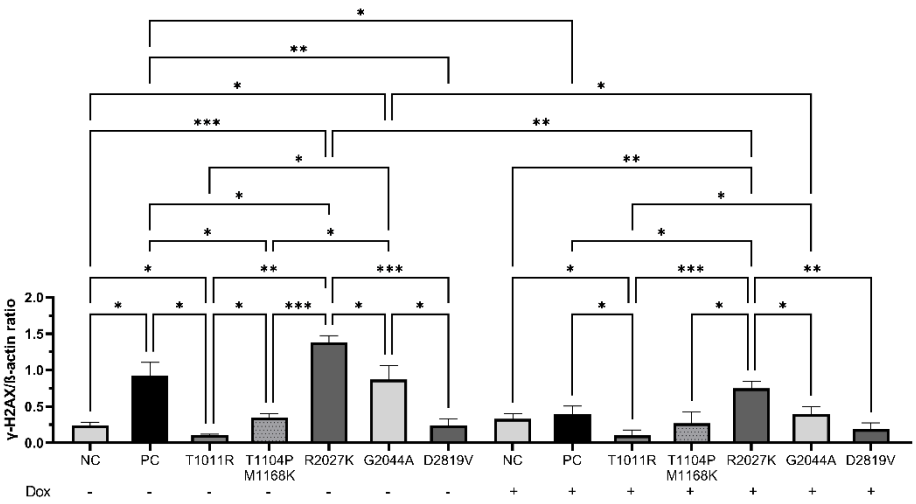

Figure 18 Comparison negative (NC) and positive (PC) controls with VUS carrier individuals prior to and following an hour long 0,5 μM Dox exposure. (α = 0,05), (* < 0,05, ** < 0,01, *** < 0,001) (16).

On the other hand, the VUS-Cs exhibited variations in the phosphorylation levels of γH2AX. Endogenous variants of uncertain significance in individuals were compared to the average value observed in normal control subjects, which was 0,2±0,04. In the study, PC levels showed a significant fourfold increase (0,9±0,2), while the P1 (T1011R) levels decreased by 40 % (0,1±0,01). Additionally, the P2 (T1104P/M1168K) levels exhibited a 2-fold increase (0,4±0,05), P3 (R2027K) showed a sixfold increase (1,4±0,09), and P4 (G2044A) indicated a fourfold increase (0,9±0,2). Notably, P5 (D2819V) did not show significant changes in this study. The average of NC individuals did not alter substantially following Dox exposure (Figure 18).

The exogenic PC (0,4±0,1) demonstrated no significant variance in contrast to the average of exogenic NC individuals (0,3±0,1) but exhibited a 40 % decrease in contrast to the endogenic PC. In a comparative analysis of exogenic VUS-Cs with the average of NC individuals, it was found that P2 (T1104P/M1168K), P4, and P5 exhibited no significant difference. However, P3 increased by 2,3-fold (0,8±0,1), while P1 decreased by 0,3-fold (0,1±0,1) following Dox-induction (Figure 18).

4.4 ATM and BRCA2 VUSs Reclassification

We classified the variants under the ACMG/AMP guideline evidence codes.

4.4.1 ATM reclassification

The classification of the *ATM* c.7793G>A was determined as VUS (+) according to the pathogenic moderate PM2 population data and pathogenic supporting PP3 in silico prediction tools. However, our functional analysis didn’t contribute to any change in the PS3/BS3 functional analysis evidence code.

4.4.2 BRCA2 reclassification

The PS3 criteria was added, which resulted in a modification in the three subjects' categorization. P5's VUS (int) became VUS (+), while P1's VUS (-) became VUS (int). Additionally, P2; (T1104P) VUS (int) became VUS (+)/M1168K is VUS (−). The P2 was finally classified as VUS (+), the reason for this is that a T1104P variation with higher pathogenicity was present. Two VUSs, P3 and P4, on the other hand, remained unchanged and were interpreted as LB.

5 DISCUSSION

This thesis comprises two projects investigating the functional characterization of missense VUSs in *ATM* and *BRCA2* genes by evaluating the damaged DNA measurement to the chemotherapeutic drugs.

The rising use of sequencing technology in familial cancer screening is recognized, highlighting the increasing demand for precise variant identification. The research emphasizes the critical role of functional studies in addressing variant categorization and conforms with ACMG/AMP guidance.

This investigation utilized a thorough methodology, integrating in silico analyses with functional assays, to gain deeper insights into the clinical consequences of single nucleotide variations in the *ATM* gene c.7793 G>A (R2598Q) and in the *BRCA2* gene c.3032C>G (T1011R), c.3310A>C/c.3503T>A (T1104P/M1168K), c.6080G>A (R2027K), c.6131G>C (G2044A), and c.8456A>T (D2819V).

We employed multiple computational tools for predicting pathogenicity, These tools offered preliminary indications regarding the possible pathogenesis of specific missense variants located in the *ATM* and *BRCA2* gene.

5.1 Discussion of the ATM Project

Following the in silico analysis, R2598Q showed higher pathogenicity scores, a significant finding. This was crucial support from PP3 evidence, but it was still classified as VUS (+). On the other hand, when we wanted to create a new evidence code with functional analyses, these analyses showed inconclusive results, and the variant's classification as VUS (+) could not be changed.

5.2 Discussion of the BRCA2 Project

As per the findings of the computational analysis, T1001R, T1104P, and D2819V exhibited higher pathogenic scores PP3 but were designated as VUSs. Conversely, R2027K and G2044A exhibited benign BP4 scores were categorized as LB.

Functional assays conducted on T1011R have revealed inconsistencies. The impact on spontaneously HR T1011R has been defined as not harmful and HR-negative (101). However, it's important to note that when the T1011R variation was expressed in yeast, no recombination activity was seen (102). Same variation additionally demonstrated reduced affinity for APRIN and RAD51 (103). Alterations in the BRC repeats genetic code may lead to BRCA2's incapacity to interact with RAD51, a vital enzyme involved in DNA recombination, ultimately hindering the process of HR repair (104). Studies have indicated that an SNV within the genetic sequence encoding the BRC1, BRC2, BRC4, and BRC7 repeats may impede their ability to bind to RAD51 (104).

According to Dines (2020), it was identified that exons 10 and 11 of the *BRCA2* gene are considered coldspots for missense variants. Remarkably, *BRCA2* exons 10–11 did not include any of the 34 pathogenic missense mutations. Additionally, it was shown that over 58.8% (3115 out of 5301) of the missense VUSs in *BRCA1* and *BRCA2* that have been published were detected within coldspots. The reclassification of these 3115 VUSs as LB would have a significant positive impact on the overall variant classification process (105). It is important to note that in our research, the exon11 variants identified as T1001R and T1104P exhibited pathogenic category as predicted by computational algorithms.

The HDR method has been accepted as a gold standard with the criteria updated by the ClinGen SVI Working Group (75). Based on this, previous findings have indicated that the D2819V variant does not function in the HDR method (106).

Comet and γH2AX analyses were employed throughout the BRCA2 study to measure the amount of damaged DNA collected in the PBMC of individuals with VUS-Cs prior to and following Dox exposure. We selected Dox as a DNA-damaging substance through diverse mechanisms and has already extensive application in cancer therapy (107). Multiple research studies have thoroughly investigated the wide range of cellular functions negatively impacted by Dox, particularly in cardiac tissue, leading to potential cardiac failure with insufficient prognoses (108). Upon exposure to Dox, the absence of BRCA2 in the cardiac tissue results in elevated levels of DNA damage, apoptosis, and impaired cardiac function (109). A controversial finding was that the MCF-7, MDA-MB 231, and T47D BC cell lines exhibited a decrease in the percentage of tail DNA following treatment with 1 μM Dox, and also ather chemotherapeutics (110). Furthermore, a reduction in tail DNA percentage was observed in colorectal cell lines following treatment with 1 μM Cisplatin (110). This observation indicated the impact of the chemotherapeutic agents on the treated cells (110). In line with Apostolou et al. findings, our study also revealed that the induction of Dox showed a reduction of DSBs in PBMCs of individuals with PC and VUS-Cs diagnosed with breast cancer.

As per the established criteria for quantifying damaged DNA, the DSBs induced by chemotherapy medications can be assessed using the Comet and γH2AX assay (111). In the initial stage, we employed the alkaline comet assay to assess damaged DNA levels prior to and following Dox exposure. It is a frequently used biological monitoring tool to evaluate the degree of damaged DNA resulting from various factors such as diet, life choice, ambient conditions, and occupational risks (112, 113). According to several research investigations, the amount of damaged DNA throughout PBMCs within individuals varies significantly (16). One study examined the impact of age, specifically before and after 60 years old (114), while another study focused on the variations among smokers based on the amount of their smoking habits (115). Another investigation observed that DNA damage in the PBMCs of healthy nonsmoker donors increased following induction with 21 nM Dox (116). Interestingly, pre-treating the cells with heat shock prior to drug

administration demonstrated a protective effect against the drug's detrimental impact (116).

The findings of this investigation reveal consistent levels of DNA in tails for both negative controls and individuals with VUS. In contrast, a rise was observed in the PC group. Notably, following Dox-induction, there was an escalation in levels observed in the healthy controls (NCs), while the other groups showed a decrease, indicating potential variations in function. This variation underscores the diversity of variants and implies that certain variants could have distinct effect on DNA repair pathway (16).

Importantly, the study demonstrated that VUS-Cs exhibited DNA damage amounts similar to NCs prior to the drug intervention. However, following Dox-induction, their DNA damage levels diminished, approaching the levels observed in the PC. Furthermore, Figure 16 illustrates an age-associated contrast (38 /58) in damaged DNA amount before and after Dox exposure between two separate negative controls, NC-1 and NC-2.

When DNA DSBs occur, the initial stage is marked by the phosphorylation of H2AX by various kinases (117, 118). Additionally, the presence of *BRCA2* heterozygous missense variants has been observed to reduce γH2AX levels following DNA damage potentially (119) a finding that raises intriguing questions about the role of BRCA2 in DNA repair. In our research, the γH2AX marker indicated noticeable variations in the amounts of DNA DSBs between individuals, emphasizing the diverse nature of the VUS landscape.

Elevated levels of γH2AX, indicating increased DSBs, were observed in P3 and P4. According to the results of in-silico prediction, these variations are deemed to be well-tolerated. These variants may explain the observed elevation by preserving complete protein activities and displaying standard quantities of H2AX phosphorylation. Nevertheless, P1, P2, and P5, exhibit diminished levels of γH2AX protein. This reduction in protein levels may suggest a decline in the structural

integrity of the intact protein. After Dox exposure, PC and VUS-Cs showed a significantly declined γH2AX amounts. This decline in damaged DNA amounts suggests the potential efficacy of dox in addressing cells with these specific mutations. The γH2AX method provided additional information to the comet method findings by assessing the amounts of the γH2AX, which is an indicator of DSBs in DNA. The identification of pathogenic variations in PC was notably linked to a significant increase in DNA damage, further establishing the pathogenic characteristics of this particular subject.

In conclusion, the consolidated evidence scores led to the reclassification of variants: P1 is considered VUS intermediate, with the presence of T1104P P2 is considered VUS plus, P5 is considered VUS plus, and P3 and P5 are considered LB.

The results of the investigation have numerous significant consequences. Functional tests are emphasized for characterizing VUS because of their importance. Although computational studies offer crucial first knowledge, the real effect of these mutations on biological functions may be intricate and situation-specific. Functional tests, like the ones employed in the present research, offer an increased awareness of VUS function. The discovered variation in damaged DNA across VUS-Cs, as indicated by changes in the tail's DNA % and amounts of γH2AX, highlights the personalized character of these genetic variants. Not every VUS has the same effects; certain may be more harmful than others, whereas others may have beneficial characteristics. The results presented here emphasize the necessity of individualized risk evaluations and therapy regimens for BRCA2 VUS patients.

The study's robustness, demonstrated in its integration of computational predictions and practical experiments, effectively connects genetic information with clinical significance, instilling confidence in the research's reliability.

The study acknowledges its shortcomings, including the limited sample size and possible biases in choosing subjects. It's important to emphasize their importance, making sure that it's clear and serving as a basis for future enhancements in research.

6 CONCLUSION

These projects significantly contribute to the current endeavors to comprehend the functional repercussions of *ATM* and *BRCA2* missense mutations.

Integrating computational predictions and experimental testing, specifically in the context of doxorubicin- and bleomycin-induced DNA damage responses, provides practical insights into the potential clinical implications of these variants for clinicians and professionals in the field.

The results emphasize the significance of personalized analysis and functional tests in interpreting genetic variations, thereby promoting the practice of personalized medicine in genetics and oncology. This will lead to more knowledgeable choices for therapy in hereditary cancer syndromes.

7 REFERENCES

1. Ho D, Quake SR, McCabe ERB, Chng WJ, Chow EK, Ding X, et al. Enabling Technologies for Personalized and Precision Medicine. Trends Biotechnol. 2020;38(5):497-518.
2. AlHarthi FS, Qari A, Edress A, Abedalthagafi M. Familial/inherited cancer syndrome: a focus on the highly consanguineous Arab population. NPJ Genom Med. 2020;5:3.
3. Rahner N, Steinke V. Hereditary cancer syndromes. Dtsch Arztebl Int. 2008;105(41):706-14.
4. Yohe S, Thyagarajan B. Review of Clinical Next-Generation Sequencing. Arch Pathol Lab Med. 2017;141(11):1544-57.
5. Rizzo JM, Buck MJ. Key principles and clinical applications of "next-generation" DNA sequencing. Cancer Prev Res (Phila). 2012;5(7):887-900.
6. Richards S, Aziz N, Bale S, Bick D, Das S, Gastier-Foster J, et al. Standards and guidelines for the interpretation of sequence variants: a joint consensus recommendation of the American College of Medical Genetics and Genomics and the Association for Molecular Pathology. Genet Med. 2015;17(5):405-24.
7. Richter S, Haroun I, Graham TC, Eisen A, Kiss A, Warner E. Variants of unknown significance in BRCA testing: impact on risk perception, worry, prevention and counseling. Ann Oncol. 2013;24 Suppl 8:viii69-viii74.
8. Federici G, Soddu S. Variants of uncertain significance in the era of high-throughput genome sequencing: a lesson from breast and ovary cancers. J Exp Clin Cancer Res. 2020;39(1):46.
9. Pesaran T, Karam R, Huether R, Li S, Farber-Katz S, Chamberlin A, et al. Beyond DNA: An Integrated and Functional Approach for Classifying Germline Variants in Breast Cancer Genes. Int J Breast Cancer. 2016;2016:2469523.
10. GM. C. The Cell: A Molecular Approach.: Sunderland (MA): Sinauer Associates; 2000. Available from: https://www.ncbi.nlm.nih.gov/books/NBK9963/. Access date: 01/04/2021
11. Bernstein C, Nfonsam V, Prasad AR, Bernstein H. Epigenetic field defects in progression to cancer. World J Gastrointest Oncol. 2013;5(3):43-9.
12. Tsaousis GN, Papadopoulou E, Apessos A, Agiannitopoulos K, Pepe G, Kampouri S, et al. Analysis of hereditary cancer syndromes by using a panel of genes: novel and multiple pathogenic mutations. BMC Cancer. 2019;19(1):535.
13. van der Groep P, Bouter A, van der Zanden R, Siccama I, Menko FH, Gille JJ, et al. Distinction between hereditary and sporadic breast cancer on the basis of clinicopathological data. J Clin Pathol. 2006;59(6):611-7.
14. Miki Y, Swensen J, Shattuck-Eidens D, Futreal PA, Harshman K, Tavtigian S, et al. A strong candidate for the breast and ovarian cancer susceptibility gene BRCA1. Science. 1994;266(5182):66-71.
15. Wooster R, Neuhausen SL, Mangion J, Quirk Y, Ford D, Collins N, et al. Localization of a breast cancer susceptibility gene, BRCA2, to chromosome 13q12-13. Science. 1994;265(5181):2088-90.

16. Ustun Yilmaz S, Agaoglu NB, Manto K, Muftuoglu M, Özbek U. Cosmic Whirl: Navigating the Comet Trail in DNA: H2AX Phosphorylation and the Enigma of Uncertain Significance Variants. Genes. 2024;15(6):724.
17. Petrucelli N DM, Pal T. BRCA1- and BRCA2-Associated Hereditary Breast and Ovarian Cancer. Seattle (WA): University of Washington, Seattle; 1993-2023.: GeneReviews® [Internet]. 1998. Available from: https://www.ncbi.nlm.nih.gov/books/NBK1247/. Access date: 01/03/2021
18. Daly MB, Pal T, Maxwell KN, Churpek J, Kohlmann W, AlHilli Z, et al. NCCN Guidelines® Insights: Genetic/Familial High-Risk Assessment: Breast, Ovarian, and Pancreatic, Version 2.2024. J Natl Compr Canc Netw. 2023;21(10):1000-10.
19. Weiss JM, Gupta S, Burke CA, Axell L, Chen LM, Chung DC, et al. NCCN Guidelines® Insights: Genetic/Familial High-Risk Assessment: Colorectal, Version 1.2021. J Natl Compr Canc Netw. 2021;19(10):1122-32.
20. Practice Bulletin No 182: Hereditary Breast and Ovarian Cancer Syndrome. Obstet Gynecol. 2017;130(3):e110-e26.
21. Wu CC, Shete S, Amos CI, Strong LC. Joint effects of germ-line p53 mutation and sex on cancer risk in Li-Fraumeni syndrome. Cancer Res. 2006;66(16):8287-92.
22. Pharoah PD, Guilford P, Caldas C. Incidence of gastric cancer and breast cancer in CDH1 (E-cadherin) mutation carriers from hereditary diffuse gastric cancer families. Gastroenterology. 2001;121(6):1348-53.
23. Riegert-Johnson D, Gleeson FC, Westra W, Hefferon T, Wong Kee Song LM, Spurck L, et al. Peutz-Jeghers Syndrome. In: Riegert-Johnson DL, Boardman LA, Hefferon T, Roberts M, editors. Cancer Syndromes. Bethesda (MD): National Center for Biotechnology Information (US) Copyright © 2009-, Douglas L Riegert-Johnson.; 2009.
24. Bubien V, Bonnet F, Brouste V, Hoppe S, Barouk-Simonet E, David A, et al. High cumulative risks of cancer in patients with PTEN hamartoma tumour syndrome. J Med Genet. 2013;50(4):255-63.
25. Antoniou AC, Casadei S, Heikkinen T, Barrowdale D, Pylkäs K, Roberts J, et al. Breast-cancer risk in families with mutations in PALB2. N Engl J Med. 2014;371(6):497-506.
26. Bogdanova N, Feshchenko S, Schürmann P, Waltes R, Wieland B, Hillemanns P, et al. Nijmegen Breakage Syndrome mutations and risk of breast cancer. Int J Cancer. 2008;122(4):802-6.
27. Cybulski C, Wokołorczyk D, Jakubowska A, Huzarski T, Byrski T, Gronwald J, et al. Risk of breast cancer in women with a CHEK2 mutation with and without a family history of breast cancer. J Clin Oncol. 2011;29(28):3747-52.
28. Goldgar DE, Healey S, Dowty JG, Da Silva L, Chen X, Spurdle AB, et al. Rare variants in the ATM gene and risk of breast cancer. Breast Cancer Res. 2011;13(4):R73.
29. Bonadona V, Bonaïti B, Olschwang S, Grandjouan S, Huiart L, Longy M, et al. Cancer risks associated with germline mutations in MLH1, MSH2, and MSH6 genes in Lynch syndrome. Jama. 2011;305(22):2304-10.

30. Loveday C, Turnbull C, Ramsay E, Hughes D, Ruark E, Frankum JR, et al. Germline mutations in RAD51D confer susceptibility to ovarian cancer. Nat Genet. 2011;43(9):879-82.
31. Loveday C, Turnbull C, Ruark E, Xicola RM, Ramsay E, Hughes D, et al. Germline RAD51C mutations confer susceptibility to ovarian cancer. Nat Genet. 2012;44(5):475-6; author reply 6.
32. Ramus SJ, Song H, Dicks E, Tyrer JP, Rosenthal AN, Intermaggio MP, et al. Germline Mutations in the BRIP1, BARD1, PALB2, and NBN Genes in Women With Ovarian Cancer. J Natl Cancer Inst. 2015;107(11).
33. Tiwari V, Wilson DM, 3rd. DNA Damage and Associated DNA Repair Defects in Disease and Premature Aging. Am J Hum Genet. 2019;105(2):237-57.
34. Fuss JO, Cooper PK. DNA repair: dynamic defenders against cancer and aging. PLoS Biol. 2006;4(6):e203.
35. Mao Z, Bozzella M, Seluanov A, Gorbunova V. DNA repair by nonhomologous end joining and homologous recombination during cell cycle in human cells. Cell Cycle. 2008;7(18):2902-6.
36. Sadeghi F, Asgari M, Matloubi M, Ranjbar M, Karkhaneh Yousefi N, Azari T, et al. Molecular contribution of BRCA1 and BRCA2 to genome instability in breast cancer patients: review of radiosensitivity assays. Biol Proced Online. 2020;22:23.
37. Zhao WT, Wang YT, Huang ZW, Fang J. BRCA2 affects the efficiency of DNA double-strand break repair in response to N-nitroso compounds with differing carcinogenic potentials. Oncol Lett. 2013;5(6):1948-54.
38. Venkitaraman AR. Cancer susceptibility and the functions of BRCA1 and BRCA2. Cell. 2002;108(2):171-82.
39. Arnold K, Kim MK, Frerk K, Edler L, Savelyeva L, Schmezer P, et al. Lower level of BRCA2 protein in heterozygous mutation carriers is correlated with an increase in DNA double strand breaks and an impaired DSB repair. Cancer Lett. 2006;243(1):90-100.
40. Zhang F, Ma J, Wu J, Ye L, Cai H, Xia B, et al. PALB2 links BRCA1 and BRCA2 in the DNA-damage response. Curr Biol. 2009;19(6):524-9.
41. Jimenez-Sainz J, Mathew J, Moore G, Lahiri S, Garbarino J, Eder JP, et al. BRCA2 BRC missense variants disrupt RAD51-dependent DNA repair. eLife. 2022;11:e79183.
42. Gatei M, Scott SP, Filippovitch I, Soronika N, Lavin MF, Weber B, et al. Role for ATM in DNA damage-induced phosphorylation of BRCA1. Cancer Res. 2000;60(12):3299-304.
43. Moslemi M, Moradi Y, Dehghanbanadaki H, Afkhami H, Khaledi M, Sedighimehr N, et al. The association between ATM variants and risk of breast cancer: a systematic review and meta-analysis. BMC Cancer. 2021;21(1):27.
44. Hettiarachchi D, Panchal H, Pathirana B, Rathnayaka PD, Padeniya A, Lai PS, et al. Six Novel ATM Gene Variants in Sri Lankan Patients with Ataxia Telangiectasia. Case Rep Genet. 2020;2020:6630300.
45. Lavin MF. Ataxia-telangiectasia: from a rare disorder to a paradigm for cell signalling and cancer. Nat Rev Mol Cell Biol. 2008;9(10):759-69.

46. Lavin MF, Scott SP, Kozlov S, Gueven N. Analyzing the regulation and function of ATM. Methods Mol Biol. 2004;281:163-78.
47. Lee JH, Paull TT. Activation and regulation of ATM kinase activity in response to DNA double-strand breaks. Oncogene. 2007;26(56):7741-8.
48. Lakin ND, Weber P, Stankovic T, Rottinghaus ST, Taylor AM, Jackson SP. Analysis of the ATM protein in wild-type and ataxia telangiectasia cells. Oncogene. 1996;13(12):2707-16.
49. Stewart GS, Last JI, Stankovic T, Haites N, Kidd AM, Byrd PJ, et al. Residual ataxia telangiectasia mutated protein function in cells from ataxia telangiectasia patients, with 5762ins137 and 7271T-->G mutations, showing a less severe phenotype. J Biol Chem. 2001;276(32):30133-41.
50. Bakkenist CJ, Kastan MB. DNA damage activates ATM through intermolecular autophosphorylation and dimer dissociation. Nature. 2003;421(6922):499-506.
51. Khanna KK, Keating KE, Kozlov S, Scott S, Gatei M, Hobson K, et al. ATM associates with and phosphorylates p53: mapping the region of interaction. Nat Genet. 1998;20(4):398-400.
52. Scott SP, Bendix R, Chen P, Clark R, Dork T, Lavin MF. Missense mutations but not allelic variants alter the function of ATM by dominant interference in patients with breast cancer. Proc Natl Acad Sci U S A. 2002;99(2):925-30.
53. Carranza D, Vega AK, Torres-Rusillo S, Montero E, Martinez LJ, Santamaría M, et al. Molecular and Functional Characterization of a Cohort of Spanish Patients with Ataxia-Telangiectasia. Neuromolecular Med. 2017;19(1):161-74.
54. Fiévet A, Bellanger D, Rieunier G, Dubois d'Enghien C, Sophie J, Calvas P, et al. Functional classification of ATM variants in ataxia-telangiectasia patients. Hum Mutat. 2019;40(10):1713-30.
55. Jacobs C, Patch C, Michie S. Communication about genetic testing with breast and ovarian cancer patients: a scoping review. Eur J Hum Genet. 2019;27(4):511-24.
56. Freedman AN, Klabunde CN, Wiant K, Enewold L, Gray SW, Filipski KK, et al. Use of Next-Generation Sequencing Tests to Guide Cancer Treatment: Results From a Nationally Representative Survey of Oncologists in the United States. JCO Precis Oncol. 2018;2.
57. Stanislaw C, Xue Y, Wilcox WR. Genetic evaluation and testing for hereditary forms of cancer in the era of next-generation sequencing. Cancer Biol Med. 2016;13(1):55-67.
58. Tung N, Lin NU, Kidd J, Allen BA, Singh N, Wenstrup RJ, et al. Frequency of Germline Mutations in 25 Cancer Susceptibility Genes in a Sequential Series of Patients With Breast Cancer. J Clin Oncol. 2016;34(13):1460-8.
59. Medendorp NM, Hillen MA, Murugesu L, Aalfs CM, Stiggelbout AM, Smets EMA. Uncertainty related to multigene panel testing for cancer: a qualitative study on counsellors' and counselees' views. J Community Genet. 2019;10(2):303-12.
60. Mighton C, Shickh S, Uleryk E, Pechlivanoglou P, Bombard Y. Clinical and psychological outcomes of receiving a variant of uncertain significance from multigene panel testing or genomic sequencing: a systematic review and meta-analysis. Genetics in Medicine. 2020.

61. Landrum MJ, Chitipiralla S, Brown GR, Chen C, Gu B, Hart J, et al. ClinVar: improvements to accessing data. Nucleic Acids Res. 2020;48(D1):D835-d44.
62. ClinVar. [Available from: https://www.ncbi.nlm.nih.gov/clinvar/. First access date: 01/04/2021, Last access date: 01/04/2024.
63. gnomAD. [Available from: https://gnomad.broadinstitute.org/. First access date: 01/04/2021, Last access date: 01/04/2024.
64. Chen S, Francioli LC, Goodrich JK, Collins RL, Kanai M, Wang Q, et al. A genomic mutational constraint map using variation in 76,156 human genomes. Nature. 2024;625(7993):92-100.
65. Kopanos C, Tsiolkas V, Kouris A, Chapple CE, Albarca Aguilera M, Meyer R, et al. VarSome: the human genomic variant search engine. Bioinformatics. 2018;35(11):1978-80.
66. engine Thgvs. [Available from: http://varsome.com. First access date: 01/04/2023, Last access date: 01/04/2024.
67. Luppino F, Adzhubei IA, Cassa CA, Toth-Petroczy A. DeMAG predicts the effects of variants in clinically actionable genes by integrating structural and evolutionary epistatic features. Nat Commun. 2023;14(1):2230.
68. Franklin. [Available from: https://franklin.genoox.com. First access date: 01/04/2023, Last access date: 01/04/2024.
69. Li C, Zhi D, Wang K, Liu X. MetaRNN: differentiating rare pathogenic and rare benign missense SNVs and InDels using deep learning. Genome Med. 2022;14(1):115.
70. Liu X, Jian X, Boerwinkle E. dbNSFP: a lightweight database of human nonsynonymous SNPs and their functional predictions. Hum Mutat. 2011;32(8):894-9.
71. Liu X, Li C, Mou C, Dong Y, Tu Y. dbNSFP v4: a comprehensive database of transcript-specific functional predictions and annotations for human nonsynonymous and splice-site SNVs. Genome Med. 2020;12(1):103.
72. Ng PC, Henikoff S. SIFT: Predicting amino acid changes that affect protein function. Nucleic Acids Res. 2003;31(13):3812-4.
73. Adzhubei I, Jordan DM, Sunyaev SR. Predicting functional effect of human missense mutations using PolyPhen-2. Curr Protoc Hum Genet. 2013;Chapter 7:Unit7.20.
74. Feng BJ. PERCH: A Unified Framework for Disease Gene Prioritization. Hum Mutat. 2017;38(3):243-51.
75. Brnich SE, Abou Tayoun AN, Couch FJ, Cutting GR, Greenblatt MS, Heinen CD, et al. Recommendations for application of the functional evidence PS3/BS3 criterion using the ACMG/AMP sequence variant interpretation framework. Genome Med. 2019;12(1):3.
76. Guidugli L, Carreira A, Caputo SM, Ehlen A, Galli A, Monteiro AN, et al. Functional assays for analysis of variants of uncertain significance in BRCA2. Hum Mutat. 2014;35(2):151-64.
77. Toland AE, Andreassen PR. DNA repair-related functional assays for the classification of BRCA1 and BRCA2 variants: a critical review and needs assessment. J Med Genet. 2017;54(11):721-31.

78. McCabe N, Turner NC, Lord CJ, Kluzek K, Bialkowska A, Swift S, et al. Deficiency in the repair of DNA damage by homologous recombination and sensitivity to poly(ADP-ribose) polymerase inhibition. Cancer Res. 2006;66(16):8109-15.
79. Boonen R, Rodrigue A, Stoepker C, Wiegant WW, Vroling B, Sharma M, et al. Functional analysis of genetic variants in the high-risk breast cancer susceptibility gene PALB2. Nat Commun. 2019;10(1):5296.
80. Guidugli L, Pankratz VS, Singh N, Thompson J, Erding CA, Engel C, et al. A classification model for BRCA2 DNA binding domain missense variants based on homology-directed repair activity. Cancer Res. 2013;73(1):265-75.
81. Starita LM, Islam MM, Banerjee T, Adamovich AI, Gullingsrud J, Fields S, et al. A Multiplex Homology-Directed DNA Repair Assay Reveals the Impact of More Than 1,000 BRCA1 Missense Substitution Variants on Protein Function. Am J Hum Genet. 2018;103(4):498-508.
82. Couch FJ, Rasmussen LJ, Hofstra R, Monteiro AN, Greenblatt MS, de Wind N. Assessment of functional effects of unclassified genetic variants. Hum Mutat. 2008;29(11):1314-26.
83. Starita LM, Young DL, Islam M, Kitzman JO, Gullingsrud J, Hause RJ, et al. Massively Parallel Functional Analysis of BRCA1 RING Domain Variants. Genetics. 2015;200(2):413-22.
84. Wu K, Hinson SR, Ohashi A, Farrugia D, Wendt P, Tavtigian SV, et al. Functional evaluation and cancer risk assessment of BRCA2 unclassified variants. Cancer Res. 2005;65(2):417-26.
85. Farrugia DJ, Agarwal MK, Pankratz VS, Deffenbaugh AM, Pruss D, Frye C, et al. Functional assays for classification of BRCA2 variants of uncertain significance. Cancer Res. 2008;68(9):3523-31.
86. Acedo A, Sanz DJ, Durán M, Infante M, Pérez-Cabornero L, Miner C, et al. Comprehensive splicing functional analysis of DNA variants of the BRCA2 gene by hybrid minigenes. Breast Cancer Res. 2012;14(3):R87.
87. Fraile-Bethencourt E, Valenzuela-Palomo A, Díez-Gómez B, Goina E, Acedo A, Buratti E, et al. Mis-splicing in breast cancer: identification of pathogenic BRCA2 variants by systematic minigene assays. J Pathol. 2019;248(4):409-20.
88. Findlay GM, Boyle EA, Hause RJ, Klein JC, Shendure J. Saturation editing of genomic regions by multiplex homology-directed repair. Nature. 2014;513(7516):120-3.
89. Findlay GM, Daza RM, Martin B, Zhang MD, Leith AP, Gasperini M, et al. Accurate classification of BRCA1 variants with saturation genome editing. Nature. 2018;562(7726):217-22.
90. Akcay IM, Celik E, Agaoglu NB, Alkurt G, Kizilboga Akgun T, Yildiz J, et al. Germline pathogenic variant spectrum in 25 cancer susceptibility genes in Turkish breast and colorectal cancer patients and elderly controls. Int J Cancer. 2021;148(2):285-95.
91. Landrum MJ, Lee JM, Benson M, Brown GR, Chao C, Chitipiralla S, et al. ClinVar: improving access to variant interpretations and supporting evidence. Nucleic Acids Res. 2018;46(D1):D1062-d7.

92. Karczewski KJ, Francioli LC, Tiao G, Cummings BB, Alföldi J, Wang Q, et al. The mutational constraint spectrum quantified from variation in 141,456 humans. Nature. 2020;581(7809):434-43.
93. Canman CE, Lim DS, Cimprich KA, Taya Y, Tamai K, Sakaguchi K, et al. Activation of the ATM kinase by ionizing radiation and phosphorylation of p53. Science. 1998;281(5383):1677-9.
94. Agilent. [Available from: https://www.agilent.com/store/primerDesignProgram.jsp. Access date: 01/03/2022.
95. PrimerX. [Available from: https://bioinformatics.org/primerx/. Access date: 01/03/2022.
96. Addgene. [Available from: https://www.addgene.org/31985/. Access date: 01/02/2021.
97. Coriell. [Available from: https://www.coriell.org. Access date: 01/03/2021.
98. Hoover RA. CometScore. 2.0 ed. http://rexhoover.com/index.php?id=cometscore. p. CometScore. Access date: 01/03/2023.
99. Ittisoponpisan S, Islam SA, Khanna T, Alhuzimi E, David A, Sternberg MJE. Can Predicted Protein 3D Structures Provide Reliable Insights into whether Missense Variants Are Disease Associated? J Mol Biol. 2019;431(11):2197-212. Access date: 01/03/2022.
100. Gudmundsson S, Singer-Berk M, Watts NA, Phu W, Goodrich JK, Solomonson M, et al. Variant interpretation using population databases: Lessons from gnomAD. Hum Mutat. 2022;43(8):1012-30.
101. Balia C, Galli A, Caligo MA. Effect of the overexpression of BRCA2 unclassified missense variants on spontaneous homologous recombination in human cells. Breast Cancer Res Treat. 2011;129(3):1001-9.
102. Spugnesi L, Balia C, Collavoli A, Falaschi E, Quercioli V, Caligo MA, et al. Effect of the expression of BRCA2 on spontaneous homologous recombination and DNA damage-induced nuclear foci in Saccharomyces cerevisiae. Mutagenesis. 2013;28(2):187-95.
103. Brough R, Bajrami I, Vatcheva R, Natrajan R, Reis-Filho JS, Lord CJ, et al. APRIN is a cell cycle specific BRCA2-interacting protein required for genome integrity and a predictor of outcome after chemotherapy in breast cancer. Embo j. 2012;31(5):1160-76.
104. Pellegrini L, Yu DS, Lo T, Anand S, Lee M, Blundell TL, et al. Insights into DNA recombination from the structure of a RAD51-BRCA2 complex. Nature. 2002;420(6913):287-93.
105. Dines JN, Shirts BH, Slavin TP, Walsh T, King MC, Fowler DM, et al. Systematic misclassification of missense variants in BRCA1 and BRCA2 "coldspots". Genet Med. 2020;22(5):825-30.
106. Richardson ME, Hu C, Lee KY, LaDuca H, Fulk K, Durda KM, et al. Strong functional data for pathogenicity or neutrality classify BRCA2 DNA-binding-domain variants of uncertain significance. Am J Hum Genet. 2021;108(3):458-68.
107. Sritharan S, Sivalingam N. A comprehensive review on time-tested anticancer drug doxorubicin. Life Sci. 2021;278:119527.
108. Nguyen HC, Frisbee JC, Singh KK. Different Mechanisms in Doxorubicin-Induced Cardiomyopathy: Impact of BRCA1 and BRCA2 Mutations. Hearts. 2024;5(1):54-74.

109. Singh KK, Shukla PC, Quan A, Desjardins JF, Lovren F, Pan Y, et al. BRCA2 protein deficiency exaggerates doxorubicin-induced cardiomyocyte apoptosis and cardiac failure. J Biol Chem. 2012;287(9):6604-14.
110. Apostolou P, Toloudi M, Kourtidou E, Mimikakou G, Vlachou I, Chatziioannou M, et al. Use of the comet assay technique for quick and reliable prediction of in vitro response to chemotherapeutics in breast and colon cancer. J Biol Res (Thessalon). 2014;21(1):14.
111. Atha DH, Reipa V. Standards for Quantitative Measurement of DNA Damage in Mammalian Cells. Int J Mol Sci. 2023;24(6).
112. Singh NP, McCoy MT, Tice RR, Schneider EL. A simple technique for quantitation of low levels of DNA damage in individual cells. Exp Cell Res. 1988;175(1):184-91.
113. Azqueta A, Ladeira C, Giovannelli L, Boutet-Robinet E, Bonassi S, Neri M, et al. Application of the comet assay in human biomonitoring: An hCOMET perspective. Mutat Res Rev Mutat Res. 2020;783:108288.
114. Singh NP, Danner DB, Tice RR, Pearson JD, Brant LJ, Morrell CH, et al. Basal DNA damage in individual human lymphocytes with age. Mutat Res. 1991;256(1):1-6.
115. Dhawan A, Mathur N, Seth PK. The effect of smoking and eating habits on DNA damage in Indian population as measured in the Comet assay. Mutat Res. 2001;474(1-2):121-8.
116. Nadin SB, Vargas-Roig LM, Cuello-Carrión FD, Ciocca DR. Deoxyribonucleic acid damage induced by doxorubicin in peripheral blood mononuclear cells: possible roles for the stress response and the deoxyribonucleic acid repair process. Cell Stress Chaperones. 2003;8(4):361-72.
117. Paull TT, Rogakou EP, Yamazaki V, Kirchgessner CU, Gellert M, Bonner WM. A critical role for histone H2AX in recruitment of repair factors to nuclear foci after DNA damage. Curr Biol. 2000;10(15):886-95.
118. Rogakou EP, Pilch DR, Orr AH, Ivanova VS, Bonner WM. DNA double-stranded breaks induce histone H2AX phosphorylation on serine 139. J Biol Chem. 1998;273(10):5858-68.
119. Krum SA, Dalugdugan EdlR, Miranda-Carboni GA, Lane TF. BRCA1 Forms a Functional Complex with γ-H2AX as a Late Response to Genotoxic Stress. Journal of Nucleic Acids. 2010;2010.

APPENDICES

APPENDIX 1 ETHICS COMMITTEE APPROVAL 1APPENDIX 1 ETHICS COMMITTEE APPROVAL 1 (CONTINUES)

APPENDIX 2 Ethics Committee Approval 2

APPENDIX 2 Ethics Committee Approval 2 (continues)

APPENDIX 3 Consent Form

APPENDIX 3 Consent Form (continues)

APPENDIX 3 Consent Form (continues)

9 CURRICULUM VITAE